6-27-2014

Separation of ash and sulfur dioxide during the 2011 Grímsvötn eruption

E. D. Moxnes
Norsk institutt for luftforskning

N. I. Kristiansen
Norsk institutt for luftforskning

A. Stohl
Norsk institutt for luftforskning

L. Clarisse
Université libre de Bruxelles (ULB)

A. J. Durant
Michigan Technological University, ajdurant@mtu.edu

See next page for additional authors

Recommended Citation

Moxnes, E., Kristiansen, N., Stohl, A., Clarisse, L., Durant, A. J., Weber, K., & Vogel, A. (2014). Separation of ash and sulfur dioxide during the 2011 Grímsvötn eruption. *Journal of Geophysical Research: Atmospheres, 119*(12), 7477-7501. http://doi.org/10.1002/2013JD021129
Retrieved from: https://digitalcommons.mtu.edu/michigantech-p/3337

Follow this and additional works at: https://digitalcommons.mtu.edu/michigantech-p

 Part of the Geological Engineering Commons, and the Mining Engineering Commons

AGU PUBLICATIONS

JGR

Journal of Geophysical Research: Atmospheres

RESEARCH ARTICLE
10.1002/2013JD021129

Key Points:
- Ash and SO_2 source terms estimated using inverse techniques and satellite data
- The transport and separation of ash and SO_2 are modeled
- Model simulations correspond well with a range of independent observations

Supporting Information:
- Readme
- Text S1
- Text S2

Correspondence to:
N. I. Kristiansen,
nik@nilu.no

Citation:
Moxnes, E. D., N. I. Kristiansen, A. Stohl, L. Clarisse, A. Durant, K. Weber, and A. Vogel (2014), Separation of ash and sulfur dioxide during the 2011 Grímsvötn eruption, *J. Geophys. Res. Atmos.*, *119*, 7477–7501, doi:10.1002/2013JD021129.

Received 1 NOV 2013
Accepted 16 MAY 2014
Accepted article online 21 MAY 2014
Published online 18 JUN 2014

Separation of ash and sulfur dioxide during the 2011 Grímsvötn eruption

E. D. Moxnes[1], N. I. Kristiansen[1], A. Stohl[1], L. Clarisse[2], A. Durant[1,3], K. Weber[4], and A. Vogel[4]

[1]Norwegian Institute for Air Research, Kjeller, Norway, [2]Spectroscopie de l'Atmosphère, Service de Chimie Quantique et Photophysique, Université Libre de Bruxelles, Brussels, Belgium, [3]Geological and Mining Engineering and Sciences, Michigan Technological University, Houghton, Michigan, USA, [4]Environmental Measurement Techniques, University of Applied Sciences, Düsseldorf, Germany

Abstract Modeling the transport of volcanic ash and gases released during volcanic eruptions is crucially dependent on knowledge of the source term of the eruption, that is, the source strength as a function of altitude and time. For the first time, an inversion method is used to estimate the source terms of both volcanic sulfur dioxide (SO_2) and ash. It was applied to the explosive volcanic eruption of Grímsvötn, Iceland, in May 2011. The method uses input from the particle dispersion model, FLEXPART (flexible particle dispersion model), a priori source estimates, and satellite observations of SO_2 or ash total columns from Infrared Atmospheric Sounding Interferometer to separately obtain the source terms for volcanic SO_2 and fine ash. The estimated source terms show that SO_2 was emitted mostly to high altitudes (5 to 13 km) during about 18 h (22 May, 00–18 UTC) while fine ash was emitted mostly to low altitudes (below 4 km) during roughly 24 h (22 May 06 UTC to 23 May 06 UTC). FLEXPART simulations using the estimated source terms show a clear separation of SO_2 (transported mostly northwestward) and the fine ash (transported mostly southeastward). This corresponds well with independent satellite observations and measured aerosol mass concentrations and lidar measurements at surface stations in Scandinavia. Aircraft measurements above Iceland and Germany confirmed that the ash was located in the lower atmosphere. This demonstrates that the inversion method, in this case, is able to distinguish between emission heights of SO_2 and ash and can capture resulting differences in transport patterns.

1. Introduction

Volcanic eruptions can inject large amounts of volcanic ash and gases (e.g., sulfur dioxide, SO_2) into the atmosphere, which can affect climate [*Textor et al.*, 2003; *Robock*, 2004], air quality [*Thorsteinsson et al.*, 2012], and local environments following fallout [*Durant et al.*, 2010]. Volcanic material injected and transported at flight altitudes is also a serious hazard to aviation [*Miller and Casadevall*, 2000; *Prata and Tupper*, 2009]. Ash can lead to dangerous aircraft engine damage, and products of SO_2 have highly corrosive properties. Satellite observations provide a unique opportunity to identify and track volcanic SO_2 and ash clouds. With the assumption that ash and SO_2 are co-emitted and transported together, SO_2 has often been used as a proxy for volcanic ash [e.g., *Carn et al.*, 2009]. However, due to different injection heights and vertical wind shear, SO_2 and ash may take different transport directions in the days following an eruption [*Holasek et al.*, 1996; *Thomas and Prata*, 2011]. For instance, *Schneider et al.* [1999] found separation of SO_2 and ash studying the El Chichón, Mexico, eruption in 1982 and *Prata and Kerkmann* [2007] distinguished between three different layers of eruption material (SO_2 layer on top and bottom, ash layer in between) in the studies of the 2005 eruption of Karthala Volcano, Comoros Islands. *Kerminen et al.* [2011] used PM10 measurements to show that a separation most likely occurred also during and after the Grímsvötn 2011 eruption, Iceland.

Modeling and forecasting the transport and atmospheric concentrations of ash and SO_2 depend critically on the knowledge of the source term. The source term includes parameters like the height of the ash- or SO_2-loaded eruption column, the mass eruption rate, and the duration of the eruption [*Mastin et al.*, 2009b]. For ash, an additional parameter is the mass fraction of fine ash (particles with diameter less than 63 μm which can remain in the cloud for many hours or days and can be transported far from the source), or more generally, the ash particle size distribution. The fine ash mass fraction can vary by more than 1 order of magnitude and is difficult to determine. Also, the vertical distribution of the ash and SO_2 in the eruption column is important. New methods for improved direct measurement of source term parameters are under

development [e.g., *Montopoli et al.*, 2013], but at present, it remains challenging to apply them globally to all types of volcanic eruptions. There are, however, several methods that can be used to indirectly derive the source term for ash and SO_2 emissions using various data and techniques. Standard volcanic ash source term parameters are specified in lookup tables from the U.S. Geological Survey [*Mastin et al.*, 2009a]. These parameters are based on mapping and characterization of ash deposits from historic eruptions but may not be representative for new eruptions. Empirical relationships between the ash mass eruption rate and observed plume heights have been derived by *Sparks et al.* [1997] and *Mastin et al.* [2009b]. These relationships are based on historical observation data and can be used to estimate the emission rate if one knows the height of the ash column. The relationships have recently been further extended to take into account atmospheric conditions such as wind or humidity [*Degruyter and Bonadonna*, 2012; *Woodhouse et al.*, 2013]. However, an assumption for the fraction of fine ash of the total mass eruption rate is still needed and remains a challenge. Furthermore, the method does not give any estimate of the vertical distribution of the ash in the eruption column. One option is to constrain the emissions from explosive eruptions to the height around the tropopause, which often acts as a barrier and leads to maximum detrainment near this height [*Durant and Rose*, 2009]. Explosive eruptions often form an umbrella-shaped cloud [*Holasek et al.*, 1996] so that using such a vertical distribution of ash emissions could be appropriate. Numerical eruption plume models such as Plumeria [*Mastin*, 2007], Active Tracer High resolution Atmospheric Model (ATHAM) [*Oberhuber et al.*, 1998], and Bent/Puffin [*Bursik*, 2001] may be "tuned" to reproduce certain aspects of the eruption and can also be used to indirectly infer source term parameters that allow fitting available observations.

Satellite observations can also be used to estimate source term parameters. The satellite instruments normally only deliver total column measurements and cannot alone provide complete information on the source term, but combined with different analysis techniques, they can also help to constrain the source height profile. One such technique that can be used to estimate the initial injection height of SO_2 and ash involves trial-and-error fits between observations of the cloud and model results obtained for different guesses of the initial injection heights [*Prata*, 2008]. The disadvantage with this method is that the model runs and observations are matched by eye, a subjective and time-consuming process. *Krueger et al.* [1996] analyzed a time series of total SO_2 mass observed by subsequent satellite measurements to determine volcanic SO_2 fluxes. The method depends on assumptions or estimates of the loss rate (or lifetime) for SO_2 and relies on satellite overpasses where the complete SO_2 cloud is observed. *Merucci et al.* [2011] used a "traverse method" to estimate SO_2 emissions based on several cross sections through a satellite-observed SO_2 plume at different distances from the volcano. With an assumption about the height of the SO_2 cloud and wind speed from meteorological data, an estimate of the SO_2 flux could be obtained. *Lopez et al.* [2012] developed a similar "box method" that uses the total observed SO_2 mass within a circle or square surrounding the volcano, the dimensions of which equal the distance the plume travels in 1 day. From this, daily SO_2 fluxes were estimated by correcting for an assumed SO_2 loss rate. All three previous methods require knowledge of the SO_2 plume height (which is often an assumption). *Eckhardt et al.* [2008] and *Kristiansen et al.* [2010] used an inverse method to determine the injection height profile of SO_2 emissions for two eruptions. Their method used satellite-observed total columns of SO_2 to constrain modeled emissions at various heights above the volcano. The inverse method was further extended by *Stohl et al.* [2011] to determine time- and height-resolved fine ash emissions for the 2010 eruption of Eyjafjallajökull. The four above mentioned methods using satellite data to derive SO_2 emission fluxes were compared by *Theys et al.* [2013] for three very different volcanic events in 2011; their Table 1 provides a valuable comparison of the four methods. Furthermore, *Flemming and Inness* [2013] used satellite retrievals of SO_2 total columns from various satellite instruments to estimate SO_2 emissions for the 2010 Eyjafjallajökull and 2011 Grímsvötn eruptions by comparing satellite observations with an ensemble of modeled test tracers injected at different heights. This method estimates the emission rates and the injection heights (not the vertically resolved profile) as a function of time. They further assimilated satellite data with the European Centre for Medium-Range Weather Forecast's (ECMWF's) four-dimensional variational data assimilation algorithm to obtain initial conditions for subsequent model forecasts. They found that plume forecasts generated using both the emission parameters and the SO_2 analyses as initial conditions provided the best forecast performance evaluated against measurements by means of hit rate and plume size statistics [*Flemming and Inness*, 2013]. *Boichu et al.* [2013] developed an inverse modeling approach that combined satellite observations with an

Eulerian regional chemistry transport model to characterize temporal volcanic SO_2 emissions during the Eyjafjallajökull eruption. In this study, the application of sequential data assimilation provided substantial improvement in the forecasts compared to an assumption of constant flux at the source. Of the above techniques, the only methodology that provides estimates of both time- and height-resolved emissions at the highest resolution is the approach taken by *Stohl et al.* [2011].

The aim of this paper is to accurately simulate the transport of both SO_2 and ash emitted during the Grímsvötn eruption in May 2011. Time- and height-resolved emissions of SO_2 and ash are estimated using the inversion method of *Stohl et al.* [2011] that integrates simulated and observed total columns of SO_2 and ash. Particular attention is given to the separation of SO_2 and ash in terms of height and time of their emissions and resulting differences in their transport. The transport simulations based on the estimated source terms are evaluated using independent observation data.

2. The Grímsvötn 2011 Eruption

Grímsvötn volcano (64.42°N, 17.33°W, 1725 m above mean sea level (msl)) is one of the most active and well-known volcanoes on Iceland. Over the past century, Grímsvötn has erupted about once per decade, the last major eruptions occurring in 1934, 1983, 1996, 1998, 2004, and 2011 (http://www.volcano.si.edu). These eruptions have typically been mafic and phreatomagmatic (interaction between water and magma) in nature, which eject large ash emissions into the atmosphere. The eruptions have often also resulted in subglacial floods (jökulhlaup) due to the location of the volcano beneath the Vatnajökull Glacier.

On 21 May 2011, the Icelandic Meteorological Office (IMO) issued a warning that volcanic tremor had been observed in Grímsvötn and that an eruption was expected to start within an hour. A few minutes later (at 19:12 UTC), a new warning was issued that the eruption had started and a moisture plume had been observed. The exact start of the eruption was not easy to determine. Volcanic status reports on a daily and even more frequent basis were issued by IMO (http://en.vedur.is/earthquakes-and-volcanism/articles/nr/2180). These reports indicate that the tremor activity at Grímsvötn associated with the eruption increased after 17:30 UTC on 21 May. The status report issued at 21 UTC informed that pilots of a passenger aircraft leaving Akureyri (northern Iceland) at 19:10 UTC flying to Reykjavik (southwestern Iceland) observed a volcanic plume after climbing to an elevation above cloud level. At approximately 19:30 UTC, they were about 60 km WNW of the plume, cruising at about 5.2 km above msl. The plume was grey with an estimated height of about 9.2 km and was rising and expanding with significant force. Several survey flights were performed by IMO on 21 May. At 20:50 UTC, it was observed that the plume was spreading at about 7.3 km height, near the tropopause. Ash was visible and falling at that height and below.

The ECMWF geopotential analysis for the 1000 hPa pressure level around the starting time of the eruption (Figure 1a) shows a low-pressure center located west of Great Britain. The corresponding wind field suggests a south and then eastward transport of material emitted to low altitudes from Grímsvötn. The analysis at 200 hPa (~11 km height; Figure 1b) shows low pressure centered west of Iceland, suggesting northwestward transport of material emitted to high altitudes. Analyses for the following 2–3 days indicated almost the same wind conditions. It is evident that there was large vertical wind shear in the atmosphere as also seen from the Skew-T, Log-p thermodynamic chart (Figure 1c) for Keflavik radiosonde station located 250 km west of Grímsvötn volcano, whereas the temporal changes of wind during the eruption period were small.

A C band weather radar at Keflavik international airport (about 250 km WSW of Grímsvötn), in addition to a mobile X band radar located about 75 km from the volcano, observed strong pulsating activity and a maximum observed ash column height of 25 km in the first few hours of the eruption [*Petersen et al.*, 2012a]. Visual photographs of the eruption plume are also available for different times [*Petersen et al.*, 2012a] and clearly show how the plume spread horizontally when it entered the very stable air of the stratosphere. Several web cameras also observed the eruption and the visible ash plumes. Lidar observations from Keflavik airport on 22 May detected low-level ash clouds [*Petersen et al.*, 2012b]. Furthermore, increased values of aerosols were observed above several sites in Scandinavia [*Tesche et al.*, 2012], Germany [*Ansmann et al.*, 2012], and Lithuania [*Kvietkus et al.*, 2012] and both SO_2 and ash plumes were clearly visible from several satellites [*Kerminen et al.*, 2011; *Tesche et al.*, 2012; *Flemming and Inness*, 2013].

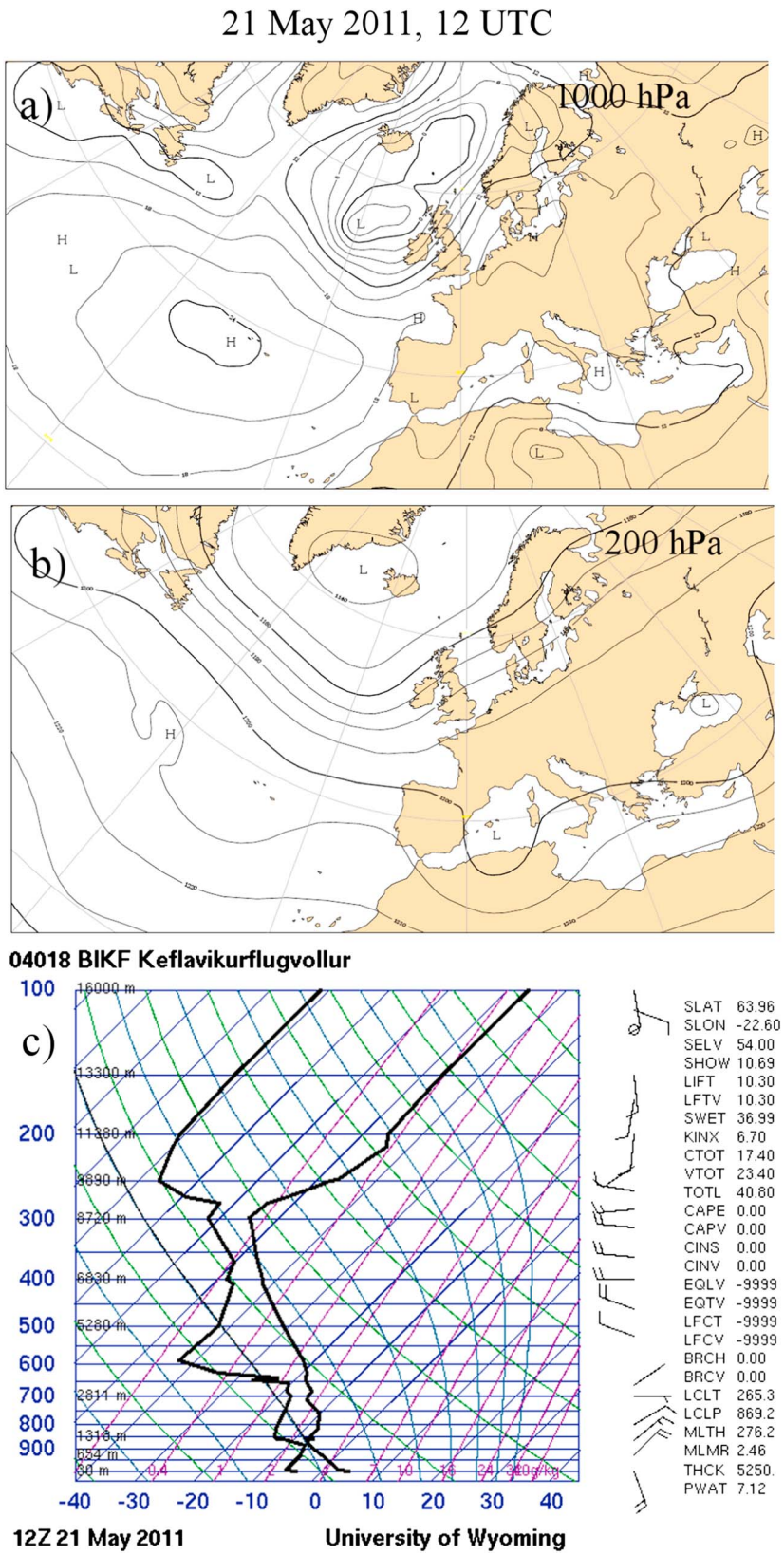

Figure 1. ECMWF geopotential analysis for 21 May 12 UTC at (a) 1000 hPa and (b) 200 hPa; data taken from http://www.ecmwf.int. (c) Skew-T, Log-p chart at Keflavik radiosonde station located 250 km WSW of Grímsvötn Volcano, at 12 UTC on 21 May 2011 (data from University of Wyoming, http://weather.uwyo.edu/upperair/sounding.html).

On 22 and 23 May, the eruption strength decreased rapidly and plume heights dropped to 5–10 km and farther below 5 km on 24 May [*Petersen et al.*, 2012a]. The eruption was officially declared over by the Icelandic Met Office at 07 UTC on 28 May (status reports, http://en.vedur.is/earthquakes-and-volcanism/articles/nr/2180). Due to the ash transported southeastward, 1% (~900 of total ~90,000) of planned flights in Europe during the period 23 to 25 May were canceled, most of them in Scotland, Northern England, Germany, and parts of Scandinavia (Global Volcanism Program reports, http://www.volcano.si.edu/reports/).

3. Methods

The inversion method applied here provides estimates for the ash and SO_2 source terms for the Grímsvötn eruption. The basic approach of the method is to determine the source terms, which bring modeled ash and SO_2 clouds in best agreement with satellite measurement data. The source terms derived with this method are "effective" emissions of SO_2 and fine ash available to long-range transport that has been observed by the satellite instruments. The method needs three types of input: a priori source term estimates, satellite observations, and model simulations. All three inputs are given for SO_2 and ash separately and are described in more detail in the following sections.

3.1. A Priori Emissions

For ash, the a priori source term needed as input to the inversion method was based on the empirical relationship between the ash mass eruption rate and observed plume heights derived by *Mastin et al.* [2009b]. The plume heights needed by this method were obtained from 5 min measurements of the fixed position C band weather [*Petersen et al.*, 2012a], averaged to 3-hourly intervals. For the times when the plume was below the radar's minimum detection height of about 6 km above msl or when no measurements were available [*Petersen et al.*, 2012a], the plume heights were set to 5.5 km above msl. The a priori ash emissions were distributed uniformly in the vertical up to the observed plume height. The ash mass eruption rate obtained by this method includes particles of all sizes. Since the inversion method only estimates the fine ash fraction of the source term, an assumed fine ash mass fraction has to be applied. An accurate number for this is, however, impossible to find. For instance, it has been suggested that there were large differences between the fine ash mass fractions emitted by the Eyjafjallajökull and Grímsvötn eruptions [*Ansmann et al.*, 2012; Icelandic Met Office, online publication, 2011]. Therefore, a pragmatic approach was used: The total amount of fine ash emitted by the eruption was set to the largest total amount of fine ash measured by the Infrared Atmospheric Sounder Interferometer (IASI), 0.4 Tg, and individual emission values were scaled accordingly. The a priori uncertainties were set high (about 100% of the highest emission values) and constant for all heights and all times. This was done to give the inversion method the same opportunity to change the emission rates at all heights and for all times. The end of a priori emissions was set to 25 May 03 UTC since no plume heights above 6 km above msl were observed by the radar after this time [*Petersen et al.*, 2012a].

As no radar heights for SO_2 exist, an independent a priori estimate for SO_2 is difficult to find. The SO_2 plume heights were therefore kept the same as those for ash, and the total a priori SO_2 mass emitted by the eruption was scaled to 0.36 Tg based on total mass estimates from IASI SO_2 retrievals. Measurements from the Ozone Monitoring Instrument and the Atmospheric Infrared Sounder are of the same order of magnitude with 0.3 Tg [*Sigmarsson et al.*, 2013] and 0.13 Tg, respectively. The a priori uncertainties for SO_2 were also set to about 100% of the highest emission values.

3.2. Satellite Data

Several satellite instruments captured the SO_2 and ash over the days following the Grímsvötn eruption. For this study, we used retrievals of the total columns of both SO_2 and ash with no vertical resolution based on infrared (IR) measurements from IASI. The data were remapped to the FLEXPART (flexible particle dispersion model) $0.25° \times 0.25°$ output grid for use in the inversion procedure.

IASI is a Sun-synchronous polar-orbiting IR sounder on board the MetOp-A satellite [*Clerbaux et al.*, 2009]. The IASI instrument has high spectral resolution and low radiometric noise and has been very useful in monitoring a host of trace gases. IASI observes in the IR spectral range 3.7–15.5 μm in 8461 channels covering three SO_2 absorption bands [*Theys et al.*, 2013] as well as volcanic ash absorption features between about 7.7 and 12.5 μm. Analyses have shown that IASI has very good sensitivity to SO_2 at high altitudes and under

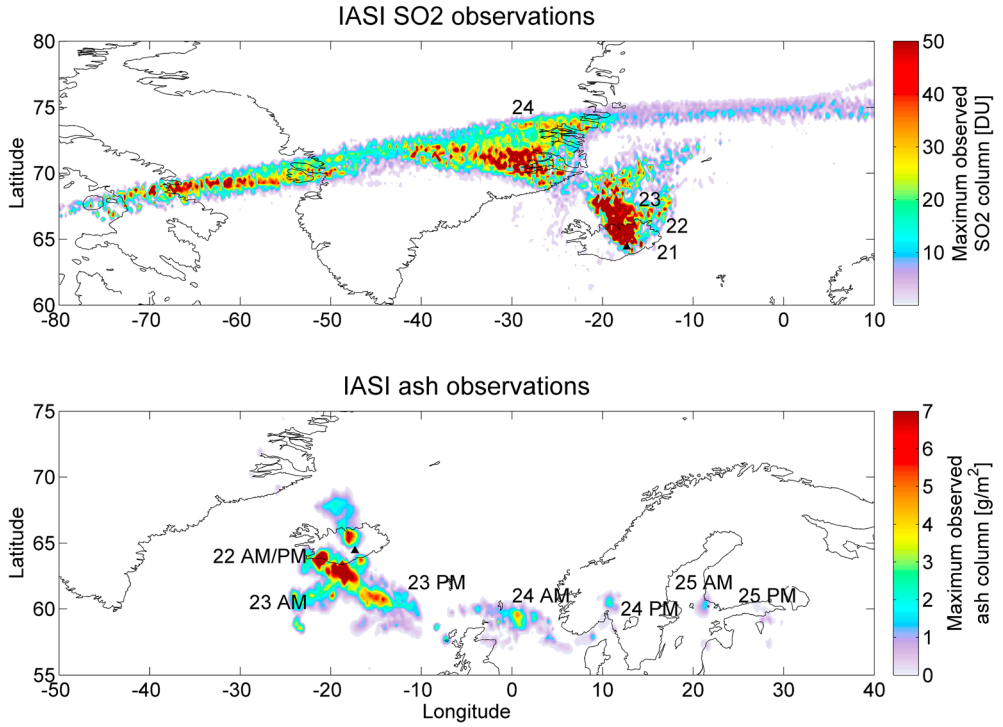

Figure 2. (top) SO_2 and (bottom) ash total columns retrieved from IASI between 21 and 24 May (SO_2) and 22 and 25 May (ash). The data are gridded and for each grid cell, the maximum of the values observed during all overpasses in the given period is shown. Labels indicate the date when the individual maxima were observed.

favorable conditions (strong thermal contrast and low water vapor content) and has limited sensitivity in the boundary layer [*Clarisse et al.*, 2008].

The SO_2 columns used were generated by the algorithm of *Clarisse et al.* [2012]. The algorithm calculates SO_2 total columns making an assumption on the altitude for the SO_2 layer. Its detection limit is dependent on many factors in the actual retrieval, but can be roughly given as 1 DU (Dobson unit). Several SO_2 products were available for six different altitudes assumptions: 5, 7, 10, 13, 16, and 25 km. Only the retrievals using the 13 km height assumption were used. This was based on analysis of the wind conditions (Figure 1) and the satellite-observed location of the SO_2 clouds as well as dispersion analysis which all indicated that the SO_2 clouds were most likely located around this height. However, the differences between the total masses for assumed cloud heights of 10, 13, and 16 km were smaller than 20%. Based on this, the uncertainties of the SO_2 satellite observations were set to 20% for the inversion.

The ash retrievals were conducted with a new retrieval algorithm. The method consists of (i) ash detection using the algorithm presented in *Clarisse et al.* [2013], (ii) simulation of a large number of different IASI spectra with different ash loading, effective radius, and height using the forward model presented in *Clarisse et al.* [2010], and (iii) matching of the observed spectra found in i with the spectra simulated in ii to obtain the best fitting values for mass, radius, and height. For the forward simulations, we used the refractive index data obtained from measurements of Eyjafjallajökull ash (D. Peters, personal communication, 2013). Height retrievals are challenging, and to minimize errors in the mass due to large errors in the retrieved height, we assumed here an ash altitude of 5 km for ash plumes detected south of Grímsvötn and 15 km for ash plumes north of Grímsvötn. These altitudes were chosen based on an initial analysis of the wind conditions (Figure 1) and the observed locations of the ash clouds. The detection limit is as for SO_2 strongly variable, but typically of the order of 0.2–0.5 g/m^2. The uncertainties of the ash satellite observations in the inversion were set to 1 g/m^2 plus 50% of the retrieved value.

Figure 2 shows composites of the SO_2 (top) and ash (bottom) columns retrieved from IASI measurements made during satellite overpasses between 21 and 24 May (SO_2) and 22 and 25 May (ash). The data are gridded and for each grid cell, a maximum over the whole period is calculated. This shows the transport of SO_2 northward and then westward over Greenland and the transport of ash first southward and then

Table 1. Satellite Observations[a]

Instrument and Detected Species	Time of Sampled Satellite Data	Number of Observations Used
IASI SO_2	22 May 11 UTC to 25 May 03 UTC	75,856 (21,379 nonzero values)
IASI ash	22 May 13 UTC to 25 May 20 UTC.	93,795 (4830 nonzero values)

[a]An overview of the time of the satellite overpasses used in the inversions. The total number of observations and the number of nonzero observation values are given for both cases.

eastward toward and across Scandinavia over the 3 days following the eruption. A summary of all the satellite data used in the inversions is given in Table 1.

3.3. Model Simulations: FLEXPART

To simulate the dispersion of volcanic SO_2 and ash, we used the Lagrangian particle dispersion model FLEXPART [*Stohl et al.*, 1998, 2005]. Except for minor differences mentioned below, the model setup was identical to the one used by *Stohl et al.* [2011] and is thus only briefly described here. For both SO_2 and ash, the simulations accounted for dry deposition [*Stohl et al.*, 2005]. For ash, the gravitational particle settling [*Naeslund and Thaning*, 1991] was determined assuming spherical particles with a density of 3000 kg/m^3, but ash aggregation was not accounted for. For SO_2, oxidation with the hydroxyl (OH) radical was considered as a sink, as in earlier studies [e.g., *Eckhardt et al.*, 2008]. FLEXPART was driven with 3-hourly meteorological data from ECMWF operational analyses with $0.18° \times 0.18°$ resolution and 91 model levels. The model output was on a $0.25° \times 0.25°$ horizontal resolution.

In this analysis, source-receptor relationships [*Seibert and Frank*, 2004] are required for the inverse modeling and describe the effect of a given source strength on the concentrations at a receptor location (here at an observation location). To establish these relationships, FLEXPART was run in forward mode for 6 days for each of the 1305 (29 three-hourly time intervals × 45 vertical layers of 0.5 km height) individual emission pulses. Three-hourly emissions between 21 May 12 UTC and 25 May 03 UTC (29 time intervals) and for 0.5 km height intervals from 0.5 to 23 km above msl (45 height layers, starting at the approximate height of the model topography) were considered and 180,000 particles were released in each model run, separately for SO_2 and ash. The simulations were started somewhat earlier than the reported start time for the eruption to see if the inversion could successfully estimate the starting time of the emissions. When simulating volcanic ash, computational particles were attributed to one of nine size bins (4, 6, 8, 10, 12, 14, 16, 18, and 25 μm diameter), which cover the size range to which the IASI satellite observations are mainly sensitive. To allow comparisons of our results with observations covering larger size ranges than the satellite data and with better size resolution, the modeled size distribution was extended both to larger and smaller sizes and using smaller size intervals for our a posteriori model runs using the inversion results.

An initial ash particle size distribution must be assumed for the ash model simulations. As a basis, an average distribution of two individual ash ground samples taken close to the volcano was used. Ground samples include all the sizes of particles that have fallen out of the ash cloud. However, for the model simulation, the size distribution needed is for the particles that are considered to take part in the long-range-transport, i.e., the smaller particles (≤25 μm diameter). Only the smallest particle sizes of the ground sample were therefore used and furthermore shifted to somewhat smaller particle sizes. The resulting initial size distribution used in the simulations is shown in Figure 16.

The model-calculated values were then compared to the satellite-observed values and scaled taking into account appropriate satellite sensitivities before being used as input to the inversion method. For ash, the sensitivity of the satellite retrievals to the size of the ash particles was accounted for following the function presented in Figure 1 of *Stohl et al.* [2011]. For SO_2, the retrieval sensitivity to the height of the SO_2 cloud affected by water vapor interference is corrected for following the averaging kernel in Figure 1 of *Theys et al.* [2013].

3.3.1. Inverse Modeling

For inverse modeling, we used the analytical algorithm of *Seibert* [2000] as described in *Eckhardt et al.* [2008] and *Kristiansen et al.* [2010] and with a very similar setup as in the study of the Eyjafjallajökull eruption [*Stohl et al.*, 2011]. The reader is referred to these papers for a full documentation of the inverse modeling. The basic idea of the algorithm is to extract information on the emission heights and times from the horizontal dispersion patterns as observed by satellite, which vary with time in response to changing emissions and

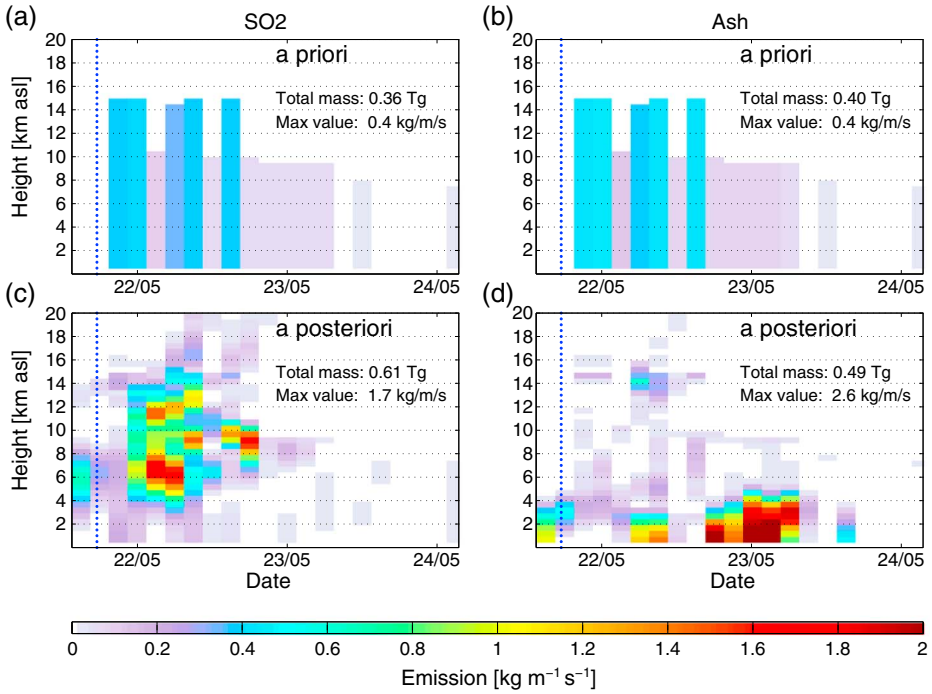

Figure 3. SO_2 and ash source terms for the 2011 Grímsvötn eruption showing the time, altitude, and strength of the emissions. (a, b) The a priori source term used as input to the inversion for SO_2 and ash. (c, d) The a posteriori source term estimated by the inversion method constrained by SO_2 and ash total columns retrieved from IASI data. The dashed blue vertical line represent the start time of the eruption as reported by IMO (21 May 2011 17:30 UTC).

changing meteorological conditions and depend on altitude because of the vertical shear of the horizontal wind. The algorithm finds the linear combination of emissions as a function of height and time, which brings the model in best agreement with the satellite measurement data. A second component of the optimization is the minimization of the deviation from the assumed a priori emissions. The two corresponding terms in the so-called cost function, which quantifies the model-measurement agreement and the deviation from the a priori emissions, are weighted against each other by the assumed uncertainties of the emissions as well as the combined observation and model error. The errors for the observation data were described in section 3.2. The model errors were in this case set to constant in both time and space. The uncertainties are propagated by the inversion algorithm into the retrieved a posteriori emissions.

4. Results

4.1. Source Term Estimates

The SO_2 source terms estimated by the inversion method are shown in Figures 3a and 3c. The total a posteriori SO_2 emissions over the time period 21 May 12 UTC to 25 May 09 UTC are estimated to 0.61 ± 0.25 Tg, which is 69% higher than our a priori emissions based on the satellite-observed total SO_2 mass. However, the total emitted mass can be substantially different from the total observed mass. This is primarily due to the conversion of SO_2 to sulfate. The lifetime of SO_2 ranges from a few days in the troposphere and up to weeks in the stratosphere [*Bluth et al.*, 1997; *Berglen et al.*, 2004], with the conversion being particularly rapid during the season when the eruption occurred. Thus, after a few days, only a fraction of the SO_2 originally emitted into the troposphere is still observable. Furthermore, SO_2 is lost from the troposphere by wet scavenging, which may be particularly important in the eruption column. The loss of SO_2 in FLEXPART takes into account removal by conversion to sulfate as well as dry deposition (which is almost negligible in this case with SO_2 at high altitudes), but does not include wet removal [*Eckhardt et al.*, 2008]. Given the simplified removal of SO_2 in the model, the a posteriori source term provides the total mass which is required to be released in the model, to best fit modeled and observed values at a later time.

The difference in inversion-derived and satellite-observed total mass is further enhanced by the decreasing instrument sensitivity to SO_2 with decreasing altitude, which means that observed SO_2 columns are systematically underestimated if a major fraction of the total SO_2 is below the 13 km reference height assumed for the retrieval (see section 3.2). The discussion below shows that this was the case for parts of the observed SO_2 cloud. Furthermore, given the filamentary and large-scale nature of the SO_2 clouds resulting from the eruption (see below), the satellite observations may have missed SO_2 transported outside the focus region or contained in filaments smaller than the satellite pixel size. All these factors suggest that SO_2 observed directly by the satellites gives an underestimation of the total emitted mass and that the higher total emitted mass obtained from the inversion might be more accurate. On the other hand, zero observation values were weighted less in the inversion than positive values, which may cause a small high bias of our a posteriori estimate. A further discussion and a more quantitative evaluation of the modeled SO_2 are given in section 4.3.1.

The time of major SO_2 emission was between 22 May 00 UTC and 22 May 18 UTC and most of the SO_2 was emitted to heights between about 5 and 13 km. Emissions reaching up to 6 km altitude start earlier than the documented start of the eruption as reported by IMO and as assumed in the a priori emissions. Considering the reported start time of the eruption at 19:00 UTC (see section 2) on 21 May, we find that about 8% (0.05 Tg) of the total emissions occurred before the reported start time. We find no evidence of such an early emission pulse in the satellite data so this is likely an artifact of the inversion.

The ash source terms estimated by the inversion method using IASI satellite data are shown in Figures 3b and 3d. The total a posteriori ash emissions were estimated to 0.49 ± 0.1 Tg, which is a 22% increase from the a priori emissions. It is important to note that total ash emissions by the Grímsvötn eruption were likely much higher. Our source terms only represent the fine ash fraction that was transported away from the volcano and was observed by the satellite instruments. The satellite instruments used are sensitive only to particles in the range between about 2 and 28 μm effective diameter; thus, only this part of the ash mass fraction of the total source term is estimated. There may have been times when ash was emitted to higher altitudes (as observed by radar, web camera, and pilot observations) and/or in larger quantities and resembled umbrella clouds. If the eruption plumes at such times collapsed and/or if the ash underwent vigorous aggregation quickly forming large particles that fell out from the atmosphere near the vent, these emissions cannot be detected by our method and are not included in the source term estimates. Thus, the ash source term derived by the inversion is the "effective" emissions of fine ash available to long-range transport that has been observed by the satellite instruments used for this study. Notice also that the 3 h time averaging used for our inversion also likely alters the umbrella cloud shape typically observed in instantaneous emission profiles.

The time period of major ash emissions was from 22 May 06 UTC to 23 May 06 UTC. The inversion again reveals an early emission pulse, which is probably an artifact of the inversion. However, the early emissions are much less prominent than for SO_2. The ash was mainly emitted to heights below 4 km, whereas there are also some small high-altitude emissions around 06–09 UTC on 22 May at 12–14 km height, colocated with the high-altitude SO_2 emissions. The inversion cannot give any information on the mechanism causing the clear vertical separation of SO_2 and ash emissions. Eruption column collapse is one likely explanation but separation between SO_2 emission and production of fine ash related to ejection dynamics is also possible.

For both the ash and SO_2 inversions, different a priori assumptions for the volcanic emission profile, eruption magnitude, and starting time were tested, and FLEXPART was also driven with different meteorological data (not shown). The source term results were quite robust to changes in both these input types. Test inversions made with preliminary data from geostationary satellite observations (SEVIRI) based on IR retrievals [*Prata and Prata*, 2012] also resulted in mainly low-altitude ash emissions occurring at about the same time as in our a posteriori source term (not shown). Details are, however, different. For instance, the break in the emissions seen during the second half of 22 May (Figures 3b and 3d) occurs 6 h later when using SEVIRI data. This indicates uncertainties in the timing of the emissions of a few hours.

Figure 4 shows the relative reduction in uncertainty of the SO_2 and ash emissions achieved by the inversion. Large uncertainty reduction indicates that the satellite observations provide a strong constraint on the emissions and small uncertainty reduction shows weaker constraint. In most cases, the error reductions are very large, indicating weak dependence of the inversion result on the a priori emissions, as also found in previous studies [*Seibert et al.*, 2011]. Especially for SO_2, the uncertainty reduction is smallest at low altitudes where the satellite sensitivity to SO_2 is smallest. It also becomes smaller toward the end of the period

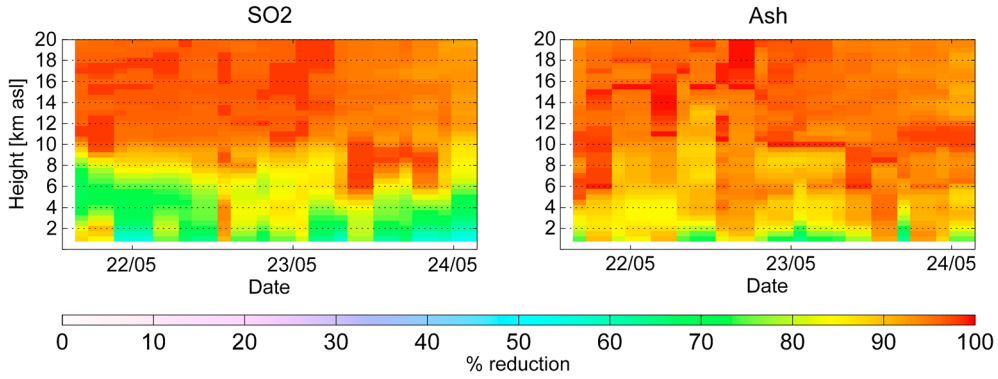

Figure 4. Relative reduction in the uncertainties of the source terms (a priori relative to a posteriori uncertainties) for (left) SO_2 and (right) ash.

considered, when fewer observational data entered the inversion. The uncertainties for the total retrieved a posteriori masses, reported above as 0.25 Tg for SO_2 and 0.1 Tg for ash, are estimated from the individual a posteriori uncertainties (shown as relative error reductions in Figure 4) but assuming an error correlation structure, with a scale height of 2 km and a scaling time of 6 h. Notice that these scaling values are subjective choices and the error covariances are not accounted for directly in the inversion. In the future, error correlations will be included directly in the inversion framework.

Based on the resulting source terms, three important differences between ash and SO_2 source terms can be stated: (1) The ash emissions occurred at substantially lower altitudes (mainly below 4 km) than the SO_2

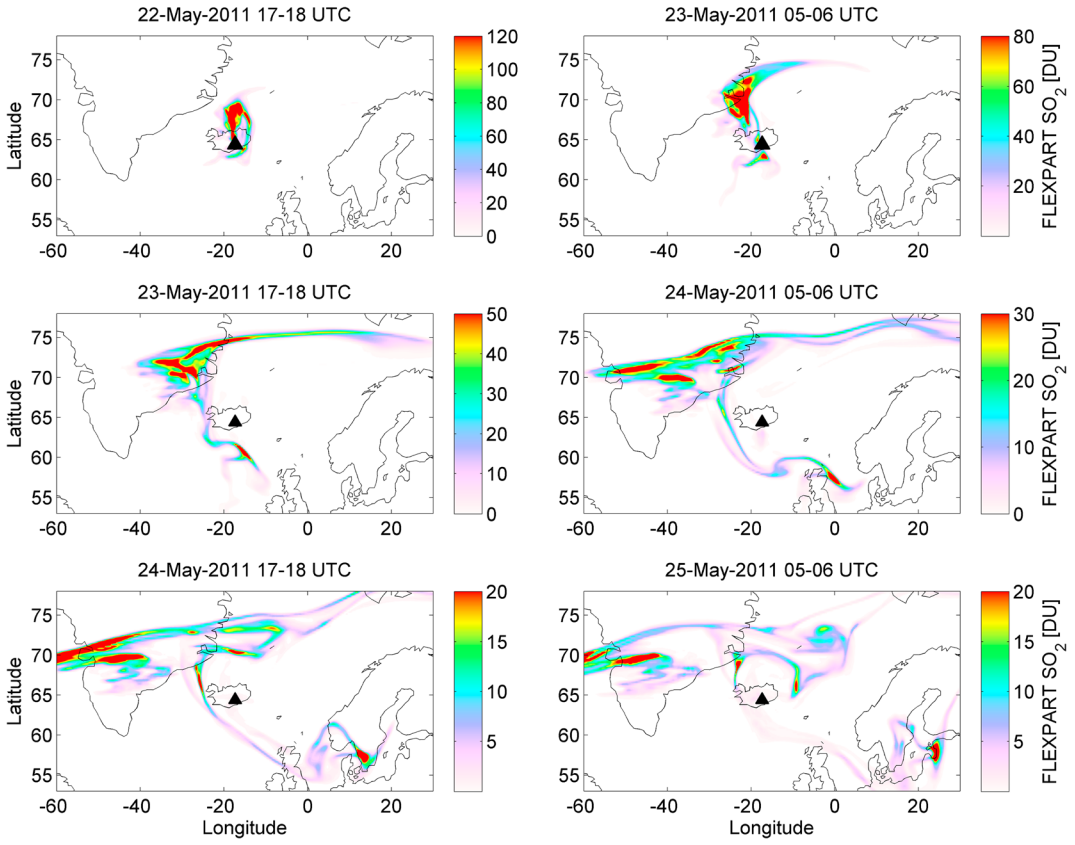

Figure 5. Total columns of SO_2 from 22 May 18 UTC to 25 May 06 UTC as simulated by FLEXPART using the SO_2 a posteriori source term. The location of the Grímsvötn volcano is marked with a black triangle. Notice the different color scales.

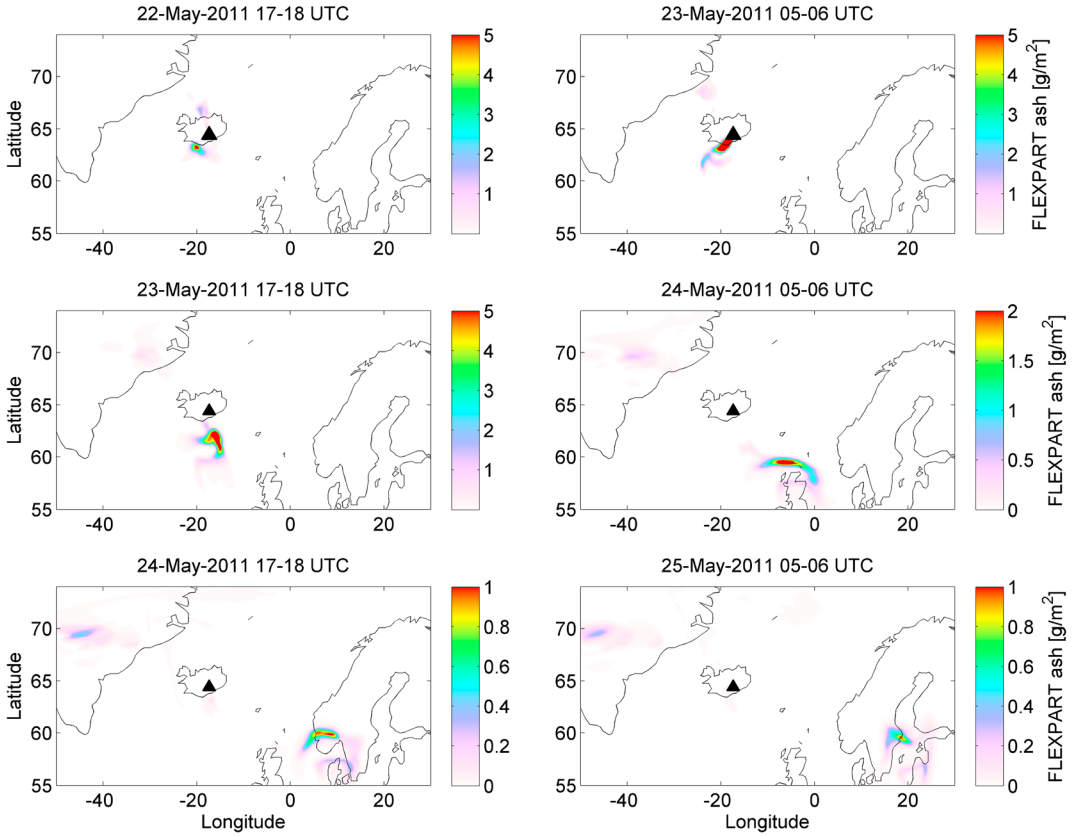

Figure 6. Total columns of volcanic ash from 22 May 18 UTC to 25 May 06 UTC as simulated by FLEXPART using the ash a posteriori source term. The location of the Grímsvötn volcano is marked with a black triangle. Notice the different color scales.

emissions (5–13 km); (2) the main ash emissions started 6 ± 3 h later than the main SO_2 emissions; and (3) the ash emissions persisted for about 6 ± 3 h longer than the SO_2 emissions.

4.2. Transport and Separation of SO_2 and Ash

In the following, we drive FLEXPART with the a posteriori source terms for SO_2 and ash to investigate their transport in the atmosphere. Total columns of simulated SO_2 and ash are shown in Figures 5 and 6 for six times between 22 May 18 UTC and 25 May at 6 UTC. On the first days (22–23 May), a large SO_2 cloud is moving northward but a smaller SO_2 cloud is also transported to the south (Figure 5). Later (24–25 May), the main part of the northerly SO_2 cloud is transported westward over Greenland. SO_2 filaments extend also northeastward toward the Svalbard archipelago. This is broadly consistent with the observed movement of the SO_2 cloud already shown in Figure 2.

In contrast, in the first days (22–23 May), almost all the ash is traveling to the south (Figure 6) while a small ash cloud is transported northward colocated with the SO_2 cloud. The southward moving ash cloud is not exactly colocated with the small southward moving SO_2 cloud due to differences in emission altitudes (Figure 3). In the later days (24–25 May), the main ash cloud moves to the southeast and then east passing north of Great Britain and western coast of Norway and then Stockholm (59.3°N, 18.1°E), very similar to the observed movement of the ash cloud shown in Figure 2.

Inspection of the vertical structure of these clouds (Figure 7) reveals that the northwestward moving SO_2 cloud is located at high altitudes, i.e., in the upper troposphere/lower stratosphere (~4–11 km above the model ground level (agl)), whereas the southeastward moving ash cloud is in the lower troposphere (below 4 km agl). These separations are caused mainly by differences in the emission altitudes for SO_2 and ash (Figure 3) but gravitational settling further reduces the altitude of the ash cloud, enhancing the differences in transport between SO_2 and ash.

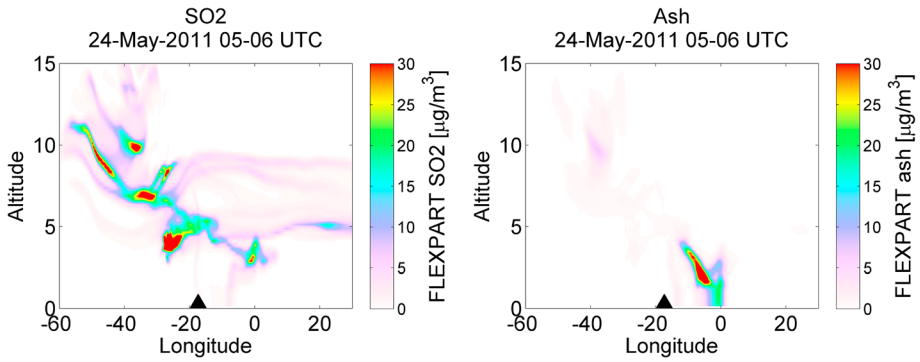

Figure 7. Cross sections of meridionally averaged (from 40°N to 80°N) mass concentrations for (left) SO_2 and (right) ash on 24 May 6 UTC.

4.3. Validation

4.3.1. Validation With Independent Satellite Data

The SO_2 results are validated by comparing the FLEXPART forward simulation based on the source terms constrained by IASI data to independent observations of the volcanic SO_2 clouds from the satellite instruments Global Ozone Monitoring Experiment 2 (GOME-2) and Scanning Imaging Absorption Spectrometer for Atmospheric Chartography (SCIAMACHY; all data taken from http://sacs.aeronomie.be/archive/). Both these instruments observe in the ultraviolet (UV) part of the electromagnetic spectrum and have much higher sensitivity to SO_2 in the lower troposphere than IASI. For direct comparison, the FLEXPART output was scaled with the SO_2 weighting function for UV instruments as given in Figure 1 of *Theys et al.* [2013].

Figure 8 shows a comparison of the a priori and a posteriori SO_2 clouds simulated by FLEXPART and the observations by SCIAMACHY around 14 UTC on 23 May. The SCIAMACHY overpass is not capturing the whole plume, so the modeled tail of the cloud going westward cannot be validated. The scatterplot (Figure 8d) and the statistical measures (for details, see *Mosca et al.* [1998]) shown in Table 2 suggest that the a posteriori model results are in relatively good agreement with the observations. Compared to the a priori simulation (Figure 8b), the bias and normalized mean square error (NMSE) between modeled and measured values are reduced suggesting that the a posteriori simulations perform better. The factor of exceedance (FOEX) indicates that underpredictions are more frequent than overpredictions, but this is reduced for the a posteriori simulations. The confidence intervals for the Pearson's correlation coefficient (PCC) also suggest the a posteriori simulations perform relatively well. It should be noted that only paired values with positive measurement values ($>$1 DU) are taken into account so that the statistical measures do not evaluate any areas where there are modeled SO_2 clouds but no observed clouds.

Figure 9 shows a similar comparison of the modeled a priori and a posteriori SO_2 cloud and observations by GOME-2 around 15 UTC on 24 May. The overall location of the westernmost SO_2 cloud stretching across the Labrador Sea seems to be well captured by the model simulations. However, the modeled cloud is covering a larger area over the southern parts of Greenland than what is observed by GOME-2 (and also by IASI, used for the source term determination; see Figure 2). The modeled SO_2 located in this area is possibly an artifact, probably due to errors in the meteorological input data. The scatterplot (Figure 9d) and the statistical comparison shown in Table 2 suggest that the a posteriori simulation is in relatively good agreement with the observations and performs better than the a priori simulation.

4.3.2. Validation With Space-based Lidar Observations

The Cloud-Aerosol Lidar with Orthogonal Polarization (CALIOP) instrument on board the Cloud-Aerosol Lidar and Infrared Pathfinder Satellite Observation (CALIPSO) satellite provides profiles of total attenuated backscatter. At 07 UTC on 25 May, the satellite passed over Greenland and made measurements in the area where the satellite-observed and modeled eruption clouds were located (Figure 10, top). The level 1 data of total attenuated backscatter at a wavelength of 532 nm (Figure 10, bottom) are compared to SO_2 and ash concentrations simulated by FLEXPART to evaluate the height of the SO_2 and ash cloud. The comparison is qualitative at best because two different quantities are compared: (i) concentration of SO_2 and ash and (ii) backscatter from particulate matter (aerosols and clouds). The observed features below 8 km are classified as

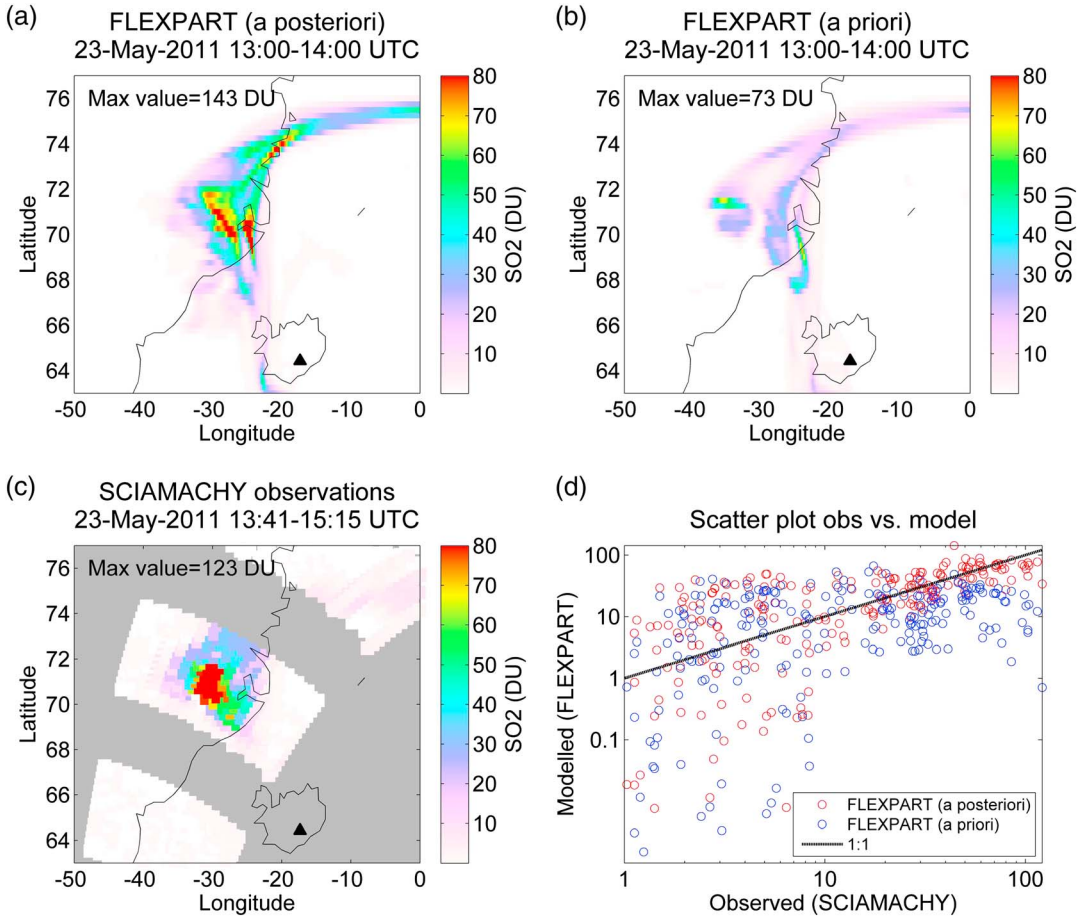

Figure 8. Comparison of modeled and observed SO_2 clouds. (a, b) The modeled SO_2 total columns as simulated by FLEXPART using the a posteriori source term and the a priori source term. The FLEXPART output is scaled with the UV satellite sensitivity given by *Theys et al.* [2013]. (c) The observed SO_2 total columns retrieved from SCIAMACHY data (non-observed areas are shown in grey) and remapped to a spatial grid of 0.25° × 0.25°. (d) A scatterplot of observed versus modeled SO_2 based on a priori emissions (blue) and a posteriori emissions (red).

Table 2. Statistical Comparison[a]

Figure 8	SCIAMACHY	FLEXPART (A Posteriori)	FLEXPART (A Priori)
Mean	19.8	21.7	11.0
Bias		2.0	−8.8
NMSE		0.7	3.1
FOEX		−11.1	−22.1
PCC conf.int.		0.69–0.80	0.19–0.41
Figure 9	GOME-2	FLEXPART (A Posteriori)	FLEXPART (A Priori)
Mean	9.3	9.6	5.0
Bias		0.3	−4.3
NMSE		1.2	3.0
FOEX		0.2	−18.0
PCC conf.int.		0.37–0.58	0.13–0.38

[a]Statistical comparison of paired modeled and satellite-observed SO_2 column loadings (DU) for the times shown in Figures 8 and 9. The modeled values are based on the a priori and a posteriori source terms, respectively. The observed values are from SCIAMACHY on 23 May 2011 and GOME-2 on 24 May 2011. Statistical measures are from *Mosca et al.* [1998]: mean of observed and modeled values, bias, and normalized mean square error (NMSE) between modeled and measured values, factor of exceedance (FOEX) in percent, and the confidence intervals (conf. int.) for the Pearson's correlation coefficients (PCC). Only paired values where observation values are over 1 DU are taken into account.

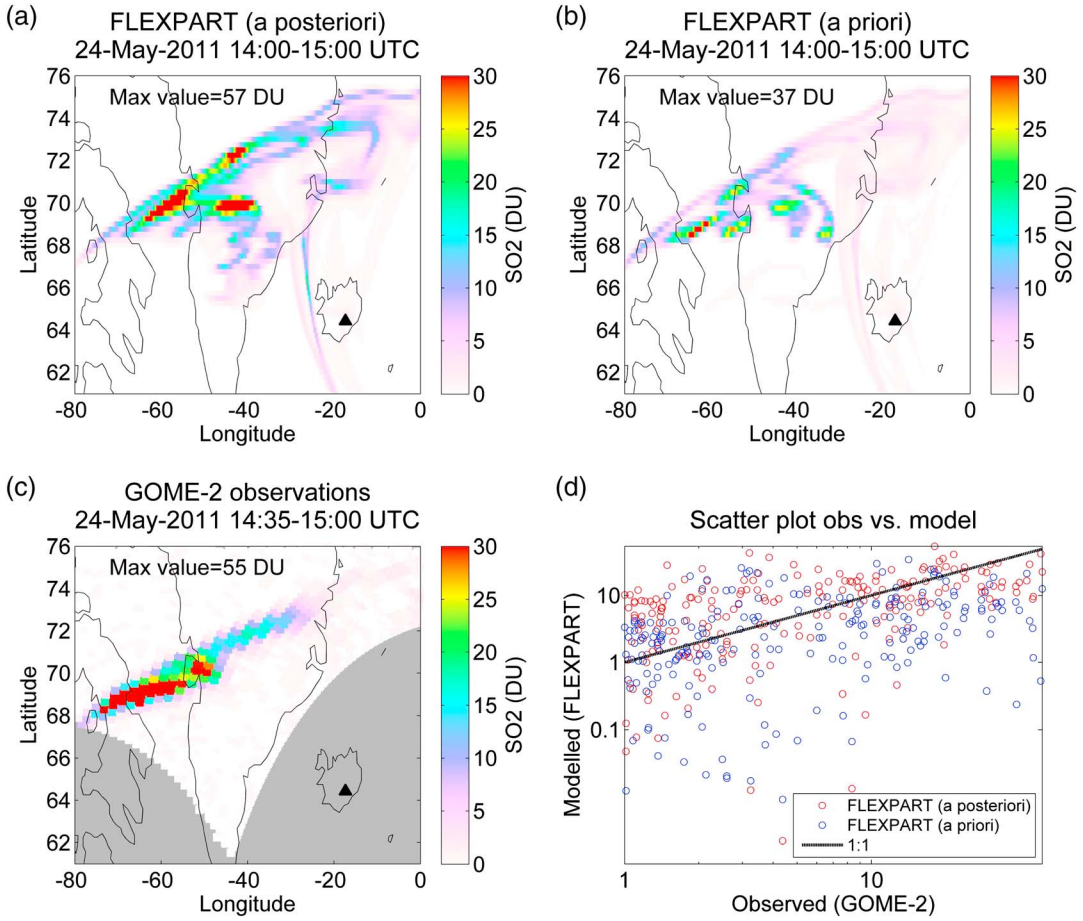

Figure 9. Comparison of modeled and observed SO_2 clouds. (a, b) The modeled SO_2 total columns as simulated by FLEXPART using the a posteriori source term and the a priori source term. The FLEXPART output is scaled with the UV satellite sensitivity given by *Theys et al.* [2013]. (c) The observed SO_2 total columns retrieved from GOME-2 data (non-observed areas are shown in grey) and remapped to a spatial grid of 0.25° × 0.25°. (d) A scatterplot of observed versus modeled SO_2 the a priori emissions (blue) and a posteriori emissions (red).

meteorological clouds in the vertical feature mask of the CALIPSO products (http://www-calipso.larc.nasa.gov/) and the observations are also somewhat noisy, due to sunlight perturbation. The features from 9 to 12 km agl height around 67–68°N are categorized as stratospheric layers (and not clouds). The modeled SO_2 and ash concentrations are located around the same latitude, but at somewhat higher altitude (10–13 km agl), although there is also a somewhat lower ash feature at about 8 km. This suggests that the layers observed by CALIOP are of volcanic origin (volcanic ash or sulfate converted from SO_2, either of which could be responsible for the backscattering, with depolarization ratio values of 0.1–0.3 not allowing a clear discrimination between the two) and that the modeled ash or SO_2 clouds are located at about the right altitude, albeit with a height difference of about 1 km. In addition to model errors, minor dislocations between the observed and modeled layers may also be due to vertically variable conversion from SO_2 to sulfate and/or gravitational settling. Unfortunately, there are no better CALIOP observations of the volcanic cloud. This is due to the sparse sampling by CALIOP but also because the formation of sulfate occurs over time scales of weeks, and thus, the sulfate concentrations just days after the eruption are fairly small and difficult to detect. Furthermore, ash concentrations in the upper troposphere/lower stratosphere, where the chances for clear CALIOP observations are largest, were very low.

4.3.3. Ash Validation With Surface Measurements

Figure 11 shows the FLEXPART simulated ash concentrations in the lowest model output layer (0–250 m agl) for particles smaller than 10 μm (PM10) using the ash a priori (see Figure 3b) and the a posteriori source term

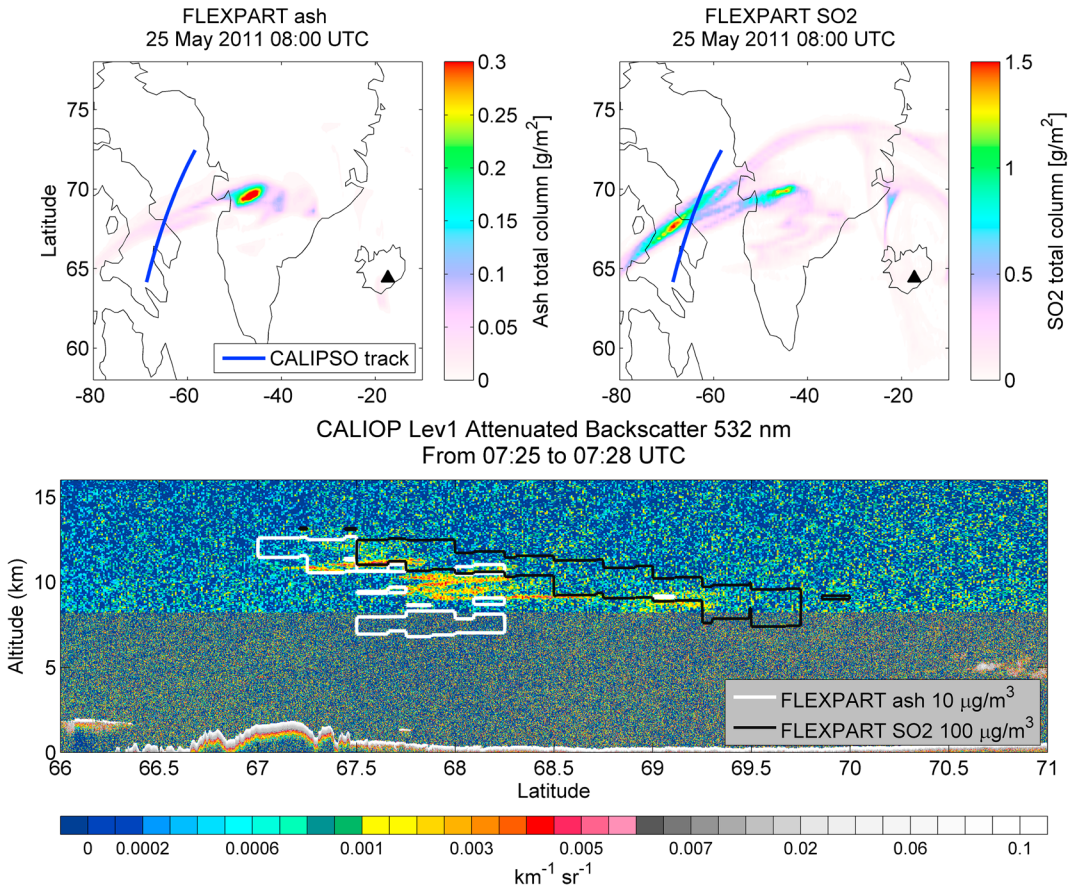

Figure 10. (top) The a posteriori modeled ash and SO_2 total columns between 07:00 and 08:00 UTC plotted together with the track of the spaceborne CALIOP lidar overflying Greenland from 07:25 to 07:28 on 25 May. (bottom) Vertical cross section along the CALIPSO track of total attenuated backscatter at a wavelength of 532 nm obtained from CALIOP (colored) superimposed with 10 $\mu g/m^3$ (white line) isolines of modeled volcanic ash and 100 $\mu g/m^3$ (black line) isolines of SO_2 concentrations from the FLEXPART simulations. The vertical layer depth of the FLEXPART-calculated concentrations is 250 m. The discontinuity of color around 8 km altitude in Figure 10 (bottom) is due to differences in resolution [see *Winker et al.*, 2009, Table 2].

(see Figure 3d) as well as PM10 surface measurements taken at five air quality monitoring stations in Scandinavia: Stavanger (59.0°N, 5.7°E) and Oslo (59.9°N, 10.7°E) in Norway, Gothenburg (57.7°N, 12.0°E) and Stockholm (59.3°N, 18.1°E) in Sweden, and Helsinki (60.2°N, 24.9°E) in Finland. It is important to notice that FLEXPART only simulates volcanic ash concentrations, whereas the PM10 measurements include also all other types of aerosols (e.g., dust, sea salt, and pollution). Based on the average of measurements before and after the volcanic episode [see *Tesche et al.*, 2012, Figure 4], a background concentration of 20 $\mu g/m^3$ was added to the FLEXPART ash modeled concentrations before comparison.

The timing of the maximum measured PM10 concentrations is well captured by the model for stations in Stavanger, Gothenburg, and Oslo, while the modeled peaks are delayed by about 6 h compared to the measured maxima in Stockholm and Helsinki. However, lower PM10 ash concentrations are simulated for the two latter stations already at nearly the same time as the first clear observed PM10 increase, suggesting that either emissions into this air mass were too low or that the simulated transport of the plume was slightly wrong. Overall, from this comparison, one may conclude that the overpass times of the volcanic ash over Scandinavia are quite well captured by FLEXPART. Furthermore, the PM10 data presented and data from other measurement sites show that the ash cloud passed Scandinavia in a relatively narrow corridor around 60°N [see *Tesche et al.*, 2012, Figure 1]. This compares well to our model simulation, which also shows the ash cloud passing mainly above this area (see Figure 6).

The maximum values of the a posteriori simulated and measured concentrations agree well at Stavanger, Gothenburg, and Helsinki stations, but the model overestimates the maximum value by a factor 2–2.5 in Oslo

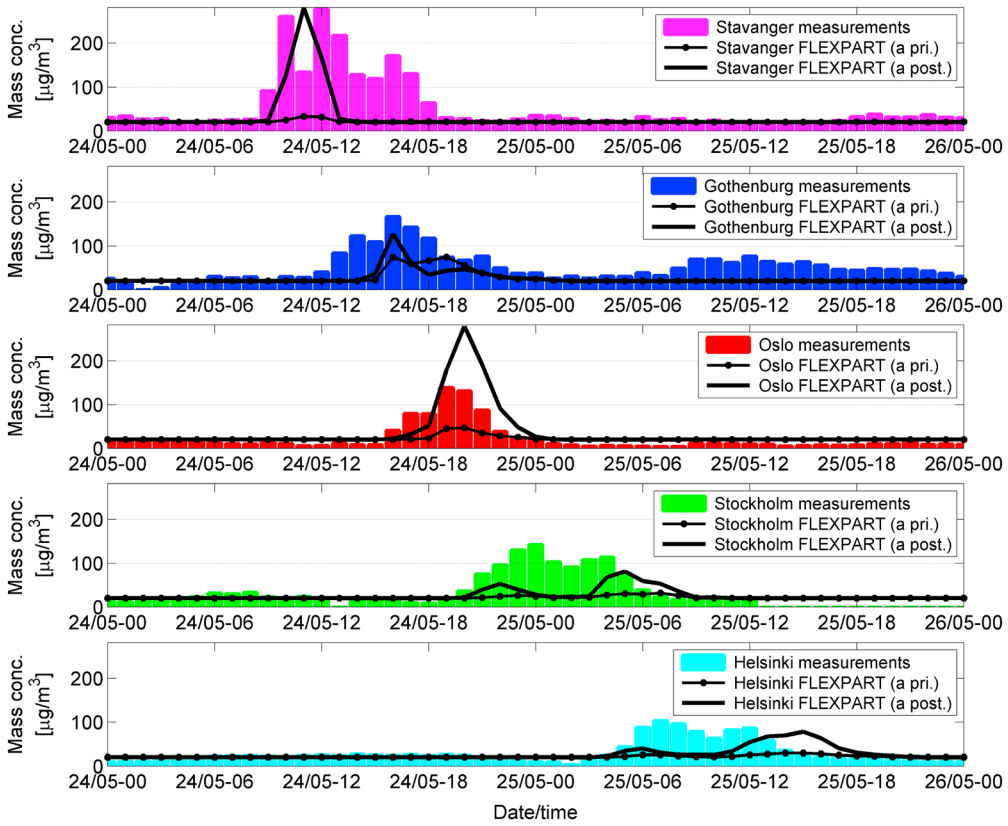

Figure 11. Hourly PM10 concentrations observed at air quality monitoring stations at five sites in Scandinavia (bar plots) and the FLEXPART-simulated PM10 concentrations of volcanic ash in the lowest model output layer (0–250 m agl) from the simulation using the a priori (dotted lines) and a posteriori (solid lines) source terms. A background concentration of 20 $\mu g/m^3$ is added to the FLEXPART concentrations.

and underestimates by about a factor 2 in Stockholm. Averaging the observed and simulated PM10 concentrations over the times of the plume passages, we find that the model underestimates by 55, 53, 47, and 24% in Stavanger, Gothenburg, Stockholm, and Helsinki, respectively. In Oslo, there is an overestimation of 41%. This results in an average low bias of 44%, averaged over all stations, which might be within the uncertainties caused by the uncertain PM10 background and the fact that we compare measured PM10 with ash-only PM10 during the episode. The a priori simulated concentrations, on the other hand, strongly underestimate the PM10 measurements at all stations. This clearly shows the improvement due to the inversion.

4.3.4. Ash Validation With Ground-Based Lidar

The simulated ash concentrations in the column above Stockholm were compared to vertically resolved lidar measurements. The lidar measures the aerosol extinction coefficients, from which the ash mass concentrations are estimated based on different assumptions about specific extinction for volcanic ash particles and the contribution of coarse particles to the total extinction measured (the coarse-mode fraction), under the assumption that the coarse mode only incorporates ash particles, for details, see *Tesche et al.* [2012]. The grey lines in Figure 12 show the hourly averaged ash mass concentrations estimated from two 30 min mean lidar profiles between 03 and 04 UTC on 25 May 2011 at Stockholm. The light and the dark grey lines represent the likely range of minimum to maximum ash concentrations as calculated by *Tesche et al.* [2012], based on a realistic range of coarse-mode fractions (0.3–0.6), and using a mean specific ash extinction of 0.64 m^2/g from the literature. The lower ash mass concentration is considered to be more reliable, in accordance with conditions observed over a lidar site at Leipzig, Germany. The peak around 1 km height is thought to be caused mainly by swollen aerosols of local origin and unscreened thin clouds near the top of the boundary layer and is therefore not volcanic ash [*Tesche et al.*, 2012].

The green and red lines in Figure 12 represent the PM10 a priori and a posteriori ash mass concentrations above Stockholm as simulated by FLEXPART for the time of the measurements. The modeled volcanic ash

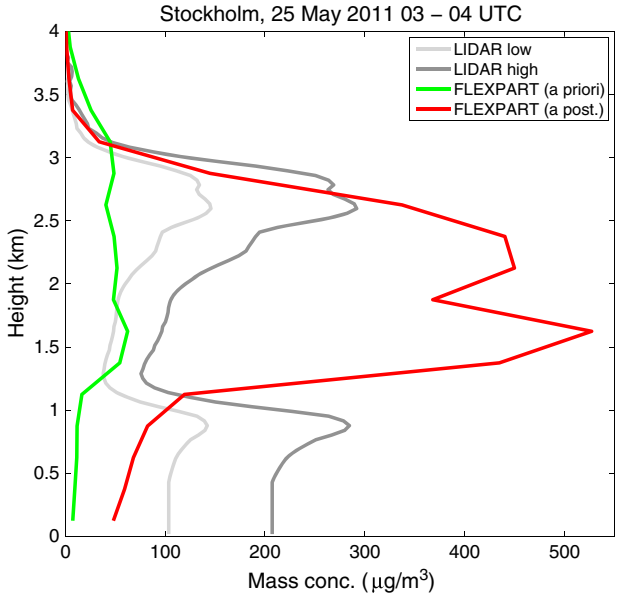

Figure 12. Minimum (light grey) and maximum (dark grey) ash mass concentrations estimated from two 30 min mean lidar profiles and the corresponding FLEXPART-simulated ash mass concentrations over Stockholm between 03 and 04 UTC on 25 May 2011. The green and red lines show the model results for PM10 when using the a priori and the a posteriori source terms, respectively. The vertical layer depth of the FLEXPART-calculated concentrations is 250 m.

layer is located between about 1 and 3 km altitude whereas the measured aerosol layer extends approximately from 2 to 3 km. Thus, there is considerable overlap between the two layers from 2 to 3 km. However, the modeled ash layer is about twice the thickness of the measured one. The modeled values using the a posteriori source term are a factor ~1.5 higher than the highest maximum estimate from the measurements and a factor ~3 higher than the lower measured estimate. However, taking into account that ash mass concentrations derived from lidar measurements are assumed to have an uncertainty of a factor of 2 [*Tesche et al.*, 2012], the agreement between the lidar measurements and the FLEXPART simulations of the volcanic ash mass is still acceptable. Note that the uncertainties in the lidar-derived ash concentrations arise from both the assumed specific extinction for ash and the assumed coarse-mode fraction, while the range of likely ash mass concentrations only consider variations in the coarse-mode fraction. *Tesche et al.* [2012] show that higher ash mass concentrations of up to 500 $\mu g/m^3$ are obtained using larger coarse-mode fractions and smaller specific ash extinction, but they are considered less likely values than those used in Figure 12. The a posteriori simulation is more conservative compared to the a priori simulation and so is more appropriate for assessment of hazards to aviation safety. The underestimate of ash aerosol concentrations near the surface is consistent with the underestimate seen in the comparison with the PM10 measurements at the same time (Figure 11; notice also that no background was added to the model results shown in Figure 12). The concentration overestimation aloft and the underestimation in the boundary layer may indicate that FLEXPART underestimates the entrainment of ash into the boundary layer in this case. When using the a priori source term, the ash concentrations are strongly underestimated by the model throughout the depth of the profile and the sharp top of the ash cloud is also not captured.

4.3.5. Validation With Aircraft Data

A total of nine measurement flights was made over Iceland between 22 and 25 May 2011 using a Cessna 206 aircraft based in Reykjavik, Iceland. These took place in cooperation between the Dusseldorf University of Applied Sciences (DUAS) and the University of Iceland. Additionally, one measurement flight was made over northern Germany on 25 May using a Flight Design CTSW (microlight/ultralight category) aircraft operated by DUAS [*Weber et al.*, 2012a]. Both aircraft are driven by piston engines and were already used during the Eyjafjallajökull eruption in 2010. They carried a Grimm 1.109 optical particle counter (OPC). The OPC combines the principles of light scattering by small particles with single particle counting to quantify airborne particulate characteristics including particle mass concentration [*Weber et al.*, 2012b]. Ambient air was sampled using an isokinetic sampling inlet and pumped inside the aircraft to the OPC measurement cell at a flow rate of 1.2 L/min. In this instrument, a fixed wavelength laser beam ($\lambda = 655$ nm) is directed through the cell and particle-scattered light is measured at two positions (29.5–150.5° and 81–99°) [*Heim et al.*, 2008]. This in turn is converted into a volume-based particle size distribution that was originally achieved using a factory-provided calibration (using monodisperse polystyrene latex spheres, refractive index $1.588 \pm 0i$). In this campaign, the OPC was configured in a second step to determine particle mass concentration in 27 size classes in the size range 0.25–63 μm diameter at a measurement interval of 6 s under assumptions of particle refractive index of $1.54 \pm 0.003i$, constant density of 2.6 g/cm^3, and spherical particles. The composition of erupted materials was classified as benmoreite and trachyte [*Gudmundsson et al.*, 2012], which represents an

intermediate silicic composition. Data on the refractive index of volcanic glass are sparse, and so a real part of the refractive index of 1.54 was used which falls within the range for andesitic glass [*Horwell*, 2007], also having an intermediate silicic composition. Under conditions of 2000 particles/cm^3, the accuracy of the measurements is ±10% [*Heim et al.*, 2008]. The OPC also collected filter samples that were later analyzed in the laboratory for single particle and bulk compositional analyses.

Comparing the measured aerosol mass from the flights with modeled ash concentrations along the flight is challenging because of differences in time and spatial scales. All flights over Iceland covered relatively small regions of the size of a few FLEXPART output grid cells only and this does not allow validating the larger-scale ash distribution simulated by the model. Subgrid variability and small position errors of the modeled ash clouds can thus lead to relatively poor agreement with the measurement data when compared point by point, and there are hardly enough data (sampling a sufficient number of FLEXPART grid cells) for statistical comparisons. The derived ash source terms and model simulations are only valid for fine ash transported away from the volcano and observed by satellite instruments. Actual ash concentrations in the volcanic cloud over Iceland at the time of the measurements were affected by processes like aggregation. The source term estimate and model simulations do not include emissions that are removed by aggregation or similar processes in the early phase of the transport and which are not observed by satellites farther downwind. Also, resuspension of deposited ash may have also influenced the measurements over Iceland, and this is also not simulated by the model. All this must be kept in mind when comparing the model with the aircraft measurements.

The first flight on 22 May around 19 UTC sampled the highest ash concentrations. The flight was conducted at a time for which the a posteriori source term indicates a break in the ash emissions (Figure 3d). Figure 13 (top) shows the flight path superimposed on a map of the mean ash mass concentrations between 500 and 1000 m agl simulated by FLEXPART using the a posteriori source term. The flight sampled only at the western edge of the simulated ash cloud. The measured aerosol mass concentrations integrated over the 1–25 μm diameter size intervals are shown in Figure 13 (bottom) along with simulated concentrations from FLEXPART using the a priori and a posteriori source terms. With both two source terms, FLEXPART simulates the decrease of concentrations as the aircraft flew westward and the increase as the aircraft turned toward the east again. Thus, the orientation of the ash plume is well captured and the measurements confirm the low altitude of the ash cloud as simulated by the model. However, the ash mass concentrations are underestimated by orders of magnitude by the model. This is due to the break in the a posteriori ash emissions, as the modeled concentrations both in the more aged plume south of Iceland and in the fresh plume closer to the volcano show concentrations similar to those observed (see Figure 13, top). Test inversions using ash retrievals from the SEVIRI instrument instead of IASI (not shown) do not produce a break in ash emissions at this time and thus give a much smaller underestimate of the ash mass concentrations along the flight track. This indicates that the break in the emissions in our a posteriori source term (Figure 3d) is too strong, occurs too early, or is an inversion artifact. If the emission break is indeed erroneous, it is probably related to missing ash detections in the air mass sampled by the aircraft (possibly downwind of where the aircraft has measured). Furthermore, some underestimate of measured concentrations close to the volcano is probably expected as our model simulations do not account for near-field processes which may efficiently remove ash in the vicinity of the volcano.

Additionally to the flight on 22 May, eight other measurement flights were conducted during the eruption period over the southwest of Iceland. Except for one flight on 23 May, all other measurement flights over Iceland were made on 24 and 25 May, after the end of the strongest volcanic emissions (compare with Figure 3). The aerosol mass concentrations measured during these flights were in general much lower than those measured on 22 May, except for a few local enhancements. The measured plumes could have been strongly influenced by ash resuspension, so a comparison with FLEXPART is not very meaningful. Overall, however, FLEXPART using the a posteriori source terms tends to underestimate these weak plumes.

Figure 14 shows the flight track for the measurement flight over northern Germany on 25 May overlaid by the modeled total column ash loadings as simulated by FLEXPART using the a posteriori source term constrained by the IASI data. FLEXPART simulates very low ash column loadings (10^{-4} g/m^2) over northern Germany at the time of the flight. Due to the short warning time after the onset of the eruption, the measurement flight could be made only after the passage of the main ash cloud, which at the time of the measurement flight,

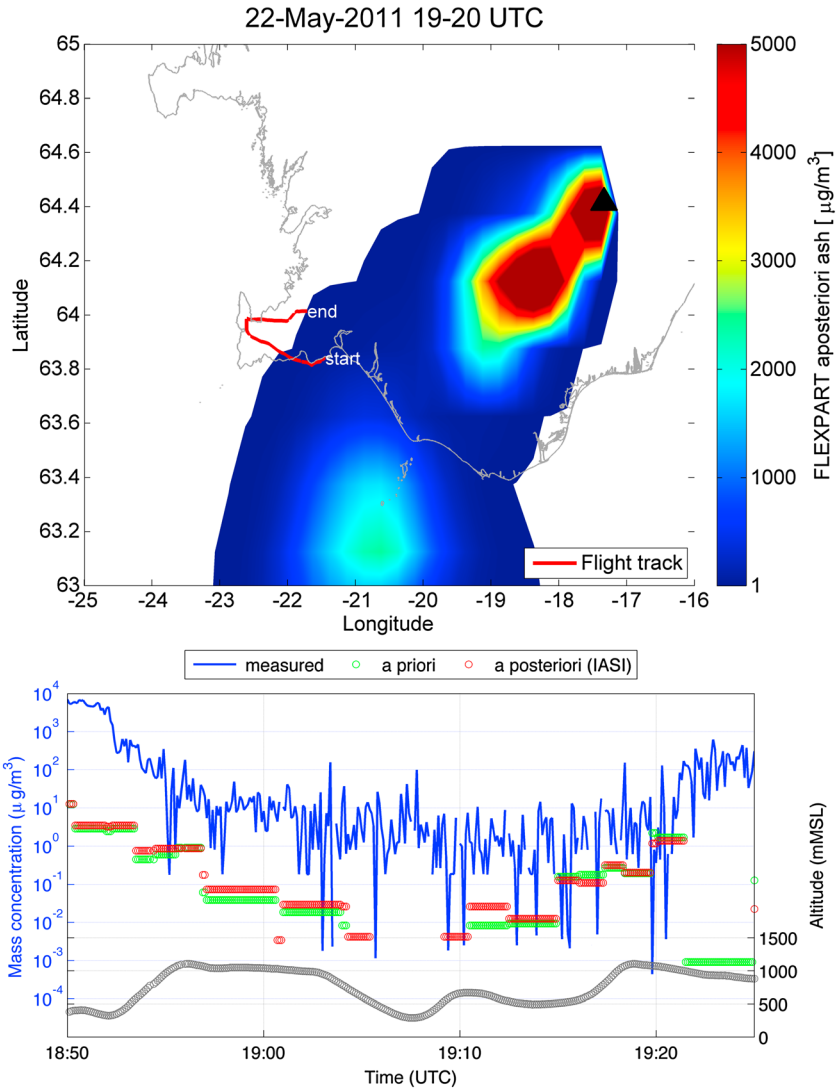

Figure 13. (top) The flight track above southwestern Iceland on 22 May 2011 between 18:50 and 19:25 UTC plotted on top of the 1-hourly averaged ash concentrations between 500 and 1000 m agl as simulated by FLEXPART using the a posteriori source term (Figure 3d). (bottom) Comparison of aircraft-measured particle mass concentrations and FLEXPART-calculated ash concentrations for particles between 1 and 25 µm in diameter. Measured particle mass concentration (blue curve), FLEXPART a priori calculated ash mass concentration (green points), FLEXPART a posteriori calculated ash mass concentration (red points), and aircraft altitude (grey points).

was already located near 20°E according to the model simulation. Furthermore, the main ash cloud passed near 60°N as seen in section 4.3.3, while the flight only reached 54°N, as northern Germany was the main area of interest for the measurement flight.

The measured atmospheric concentration of particles in the size range 1–25 µm diameter (Figure 14, bottom, blue curve) was highly variable, with values ranging typically from a few 10^{-1} to mostly values of 0.5×10^{2} µg/m^3. High measured particle concentrations at the start and end of the flight were likely due to local particulate sources at lower altitudes in the atmospheric boundary layer. At higher altitudes, a thin optically opaque layer was observed from the cockpit, which was subsequently penetrated by the aircraft. The OPC filter was analyzed after the flight using scanning electron microscope (SEM)–electron dispersive X-ray spectroscopy. A proportion of the particles had a morphology that resembles volcanic ash (angular, shard like) and composition that was within the range measured for Grímsvötn ash fallout collected close to the volcano (B. Groberty, University of Fribourg, personal communication, 2013) and farther downwind [*Lieke et al.*, 2013]. Some nonvolcanic aerosols were also found in the SEM analysis, which are thought to have been

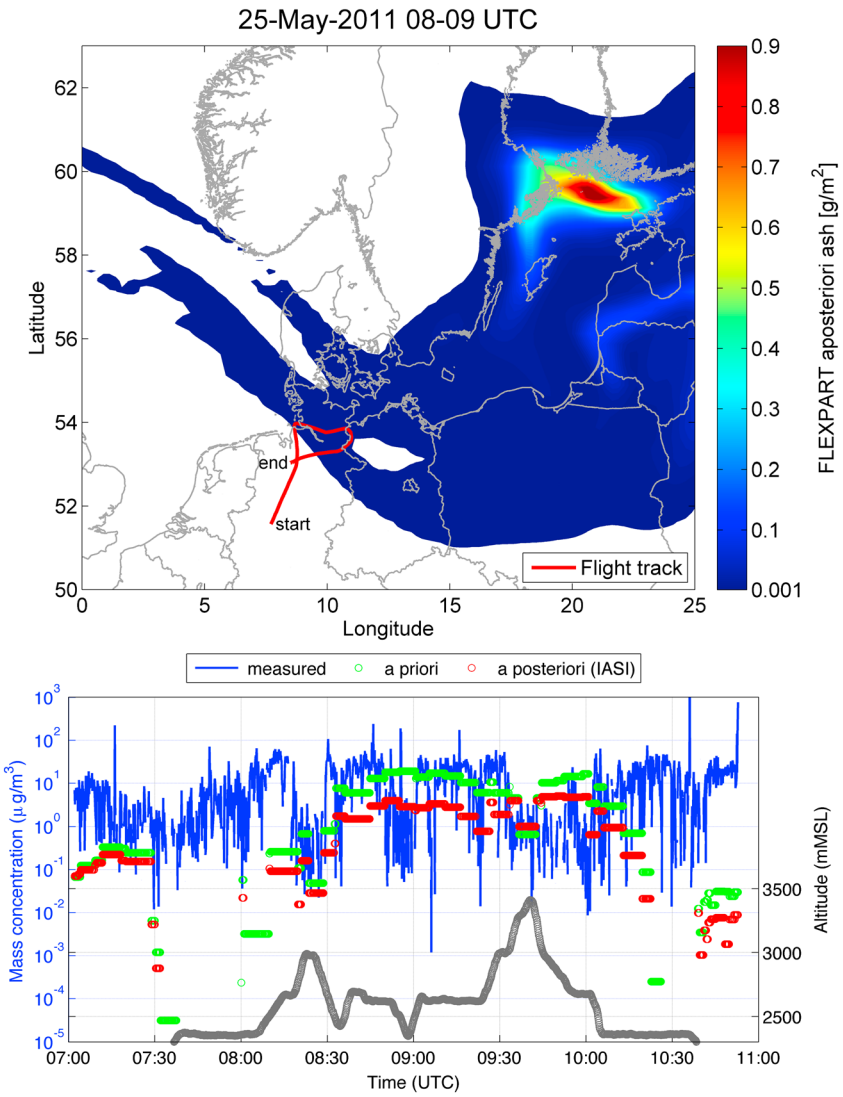

Figure 14. (top) The flight track above Germany on 25 May 2011 between 07:00 and 11:00 UTC plotted on top of the 1-hourly averaged total ash loadings as simulated by FLEXPART using the a posteriori source term. (bottom) Comparison of aircraft-measured particle mass concentrations and FLEXPART-calculated ash concentrations for particles between 1 and 25 μm in diameter. Measured particle mass concentration (blue curve), FLEXPART a priori calculated ash mass concentration (green points), FLEXPART a posteriori calculated ash mass concentration (red points), and aircraft altitude (grey points).

captured during the climb and descent phases of the flight. However, the SEM analysis builds confidence that volcanic ash was indeed sampled and measured during the flight. Furthermore, the measured particle concentrations are still much higher than expected for the background atmosphere at altitudes above 2.5 km, which in turn, together with the SEM analysis and the visual plume observation, give strong indications that volcanic ash was measured at higher altitudes.

The a priori FLEXPART ash concentrations (Figure 14, bottom, green points) were higher than the a posteriori FLEXPART ash concentrations (red points) and show a closer agreement with the measured aerosol concentrations. This relates to the constraints of the a posteriori source term from the satellite data. Like for the later flights over Iceland, IASI did not observe any ash in the air mass sampled by the aircraft at any time, as the ash column loadings are below the detection limit. Therefore, the inversion decreased the a priori emissions into this air mass. It is possible that this decrease, due to the limited sensitivity of the satellite instruments to low ash loadings, was not correct, demonstrating difficulties to quantitatively model low ash concentrations. It is noted, however, that the resulting ash mass concentrations are too small to be of concern for aviation or air quality.

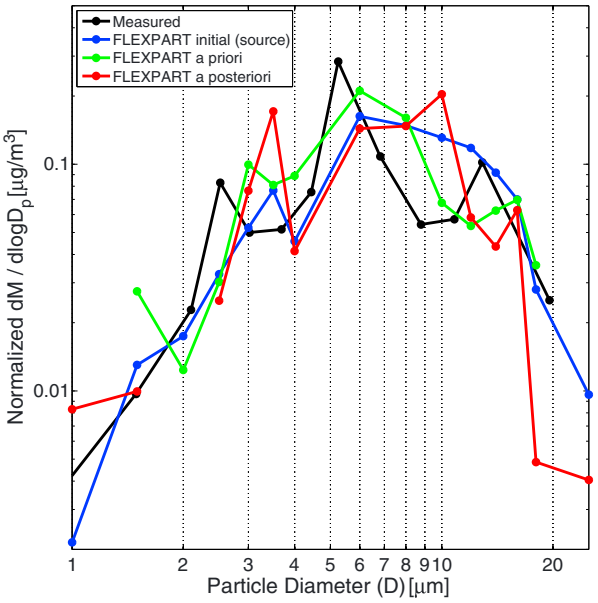

Figure 15. Measured (black line) and modeled (red and green lines) normalized particle mass size distributions measured by the Cessna 206 aircraft on 22 May 2011 over Iceland. The measurements are from a time when the aircraft was near the maximum altitude during the early part of the flight at 18:56 UTC. The measured size distribution is an average of 84 measurements (taken every 6 s) to obtain an average comparable to the horizontal resolution of the model. Also shown is the initial particle size distribution used in the model at source (blue line).

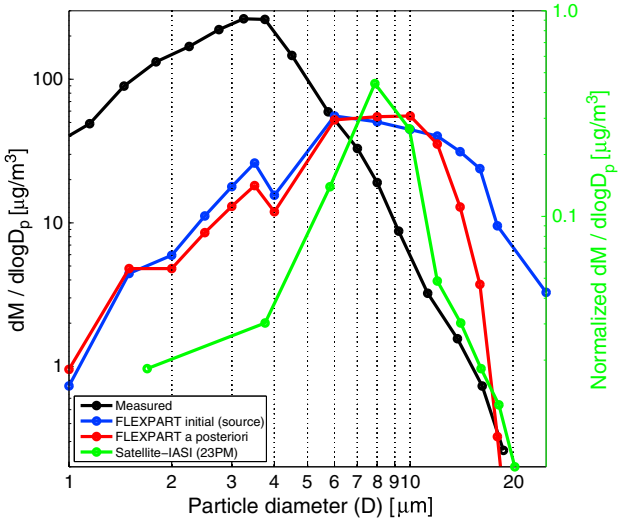

Figure 16. Measured (black line) and modeled (red line) particle mass size distributions at Stockholm between 24 May 2011 22 UTC and 25 May 2011 06 UTC. Also shown are the assumed initial particle size distribution injected into the model atmosphere at the source (blue line) and a normalized distribution of particle effective diameters derived from our IASI retrievals on 23 May PM for the ash cloud southeast of Iceland (green line, right axis).

4.3.6. Ash Size Distribution Validation

Ash particle size distributions from the 1-hourly averaged model output were compared with measured size distributions from two different observation data sets: from the OPC mounted on the Cessna 206 aircraft measuring the close-to-source ash over Iceland on 22 May and from a ground-based OPC at Stockholm measuring the more dispersed ash cloud on 25 May.

The normalized particle size distribution from the Cessna 206 aircraft measurements taken over Iceland on 22 May is shown in Figure 15 (black line). The measured size distribution peaks around 5 µm. The overall shape of the modeled ash particle size distributions using the a priori (green) and a posteriori (red) source emissions, as well as the ash size distribution emitted at the source (blue line; notice that this size distribution was used for initializing both the a priori and a posteriori simulations), are very similar to the shape of the measured one.

The particle mass size distribution obtained by an optical particle counter in Stockholm (details given in *Tesche et al.* [2012]) is shown in Figure 16 together with the modeled size distribution from the FLEXPART a posteriori simulations and the normalized particle size distribution derived from IASI data on 23 May PM for the ash cloud southeast of Iceland. Only ash particles with diameter larger than 0.5 µm are simulated by the model. Smaller particles are likely mainly sulfate which is not simulated. The measured particle size distributions should be considered as approximate with an uncertainty of at least a factor of 2 [*Tesche et al.*, 2012].

The measured size distribution at Stockholm (black line) peaks near 4 µm diameter, while the FLEXPART modeled size distribution (red line) has a broad peak between 6 and 10 µm. Thus, the modeled size distribution is shifted to larger particle sizes relative to the observed one. *Tesche et al.* [2012] report that the measured peak might be located at larger diameters due to possible losses of larger particles in the inlet system. The

particle size distribution obtained from the IASI retrievals (blue line), albeit taken from a region closer to the volcano than Stockholm, peaks at 8 μm, which is in fairly good agreement with the modeled maximum, except that the size distribution obtained from IASI is narrower than all other size distributions. This is to be expected as the IASI algorithm retrieves an effective diameter per pixel, representative assuming a lognormal size distribution with a prefixed spread. Effective radius data are routinely reported by satellite retrievals; however, it is not straightforward to compare these data with modeled or in situ measurements of mass size distributions. Thus, caution should be taken when drawing conclusions from such a comparison alone.

The modeled particle size distribution clearly depends on the chosen initial particle size distribution at the source (shown as the green line in Figure 16) and on the assumed particle density which influences gravitational settling and deposition, as also shown by *Dacre et al.* [2013] for the Eyjafjallajökull eruption. In the model simulations, the initial particle size distribution at the source is constant throughout the whole eruption period. This is a simplification and probably not realistic considering the complexity of the eruption. As can be seen by the difference between the blue and red/green lines in Figure 16, the gravitational settling has removed most of the particles larger than about 10 μm but the size distribution for smaller particles in Stockholm is virtually unchanged from the initial distribution. Also, gravitational settling followed by differential advection in the presence of vertical wind shear can contribute to the particle size measurements at specific locations downstream [*Dacre et al.*, 2013]. In reality, other processes such as ash aggregation shape the size distribution as well, and this is not simulated by the model. This may lead to a too slow removal in the model of particles that are too small to be directly removed by gravitational settling but which could easily be removed after aggregation. However, it must also be noticed that the real peak in the measurements might actually be located at larger sizes due to possible losses of larger particles in the inlet system of the instrument [*Tesche et al.*, 2012]. Still, as also in *Kristiansen et al.* [2012], the modeled ash particle size distribution was shifted to larger sizes in the model compared to the observations and this may point toward a wrong initial size distribution or missing processes in the model and should be further investigated.

5. Conclusions

For the first time, an inversion method was used to estimate the individual source terms for both SO_2 and ash from a volcanic eruption. This was done by using total column measurements of SO_2 and ash from satellite instruments and a Lagrangian dispersion model, FLEXPART, as well as a priori estimates for the source terms. The method was applied to the eruption of Grímsvötn volcano in May 2011.

The source terms for SO_2 and ash were obtained by using satellite observations from the IASI satellite instrument from up to 4 days after the eruption onset. The inversion method estimates a total a posteriori source of 0.61 ± 0.25 Tg of SO_2 emitted mostly to 5–13 km altitude during 22 May and 0.49 ± 0.1 Tg of fine volcanic ash (2–28 μm in diameter) emitted mainly to heights below 4 km during 22 and 23 May. Some small amounts of ash were also emitted to higher altitudes, to the same height, and in the same time period as SO_2. It is important to notice that the total amount of ash retrieved with our method represents only the fraction of ash undergoing long-range transport in the atmosphere. Much larger amounts of ash were removed from the atmosphere locally by the joint rapid action of processes such as coagulation, take-up in ice hydrometeors, gravitational settling, and precipitation scavenging.

The transport of SO_2 and ash was simulated with FLEXPART using the a posteriori source terms. The model simulated a clear separation of SO_2 and ash with the SO_2 first moving north and then westward and most of the ash first moving south and then eastward.

The SO_2 model simulations showed reasonable agreement with independent satellite observations from the GOME-2 and SCIAMACHY instruments and a clear statistical improvement of the simulations due to the inversion. Furthermore, a qualitative comparison of both the SO_2 and ash concentrations and observations from an overpass of Greenland by the CALIOP spaceborne lidar showed measured aerosol layers and modeled SO_2 and ash layers at about the same latitude and height.

The ash model simulations also compared well with surface and lidar measurements at stations in southern Norway, Sweden, and Finland. The simulated ash cloud arrived at the measurement sites at exactly the same time as significant increases in the surface observations of PM10 were observed for the westernmost stations, but the simulated ash cloud was delayed by about 6 h for the stations farther to the east. The surface

concentrations were well reproduced in the simulations with an average low bias of 44%, while the ash concentrations in Stockholm at heights 1–3 km were somewhat overestimated. The ash particle size distribution was shifted to too large particles (maximum at 6–10 μm) compared to observations in Stockholm (maximum at 4 μm) but was in fairly good agreement with effective diameter distributions obtained from the IASI retrievals.

Comparisons were also made with aerosol mass concentration measurements obtained during measurement flights over Iceland and northern Germany. The flights only covered small areas not much larger than a few model output grid cells and, over Iceland, were influenced by processes like aggregation and resuspended ash which are not simulated, all of which make comparisons with model results difficult. The model captured the spatial ash gradients well for this flight but underestimated the ash concentrations due to a break in the a posteriori emissions before the flight, which was probably not real. The only flight over Germany was carried out in an air mass with relatively low aerosol mass concentrations. The a posteriori FLEXPART simulation showed lower ash mass concentrations than measured which was due to the constraint of the source term by the satellite data, which did not observe any ash in the area. The resulting ash concentrations were, however, too low to be of concern for aviation or air quality.

We make our source terms available as the supporting information to this publication. While the source terms were determined with relatively high vertical (500 m) and time (3 h) resolution, the exact time intervals or altitudes of emission maxima are somewhat sensitive to the parameter settings in the inversion. For instance, the research flight over Iceland on 22 May indicates that the break of the volcanic ash emissions on 22 May occurs at the wrong time or may be an inversion artifact. Thus, for certain applications, it may be advisable to use smoothed versions of these source terms. We also point out that the ash source terms derived are for fine ash transported away from the volcano and observed by satellite instruments only. Total ash emissions by the Grímsvötn 2011 eruption were likely much higher but most of this ash was deposited in the vicinity of the volcano.

The method demonstrated in this paper can be used to estimate the emissions of volcanic ash and SO_2 to the atmosphere and to more accurately simulate the transport of volcanic emission clouds. This can aid aviation in case of volcanic clouds intersecting air traffic routes and be used in climate applications that evaluate potential climate impacts of large volcanic eruptions.

Acknowledgments

This work was partly funded by the European Space Agency thought the project Volcanic Ash Strategic initiative Team (VAST, ESA-ESRIN contract 4000105701/12/I-LG). L.C. is postdoctoral researcher (Chargé de Recherches) with the F.R.S.-FNRS. We thank Matthias Tesche at Stockholm University, Department of Applied Environmental Science, for providing measurement data from Stockholm and other Scandinavian stations used for validation. We thank Kerstin Stebel at NILU for help with CALIOP data. We would like to thank Daniel Peters from the University of Oxford for the refractive index data of Eyjafjallajökull ash. We thank Jonas Eliasson from the University of Iceland for scientific cooperation during the flights over Iceland. The partial funding of the flights over Iceland by the Icelandic flight provider ISAVIA is greatly acknowledged as well as the partial funding of the flight over Germany by the German Weather Service DWD and the German Federal Ministry of Transport, Building and Urban Development.

References

Ansmann, A., P. Seifert, M. Tesche, and U. Wandinger (2012), Profiling of fine ash and coarse particle mass: Case studies of Saharan dust and Eyjafjallajökull/Grímsvötn volcanic plumes, *Atmos. Chem. Phys.*, *12*, 9399–9415, doi:10.5194/acp-12-9399-2012.

Berglen, T. F., T. K. Berntsen, I. S. A. Isaksen, and J. K. Sundet (2004), A global model of the coupled sulfur/oxidant chemistry in the troposphere: The sulfur cycle, *J. Geophys. Res.*, *109*, D19310, doi:10.1029/2003JD003948.

Bluth, G. J. S., W. I. Rose, I. E. Sprod, and A. J. Krueger (1997), Stratospheric loading of sulfur from explosive volcanic eruptions, *J. Geol.*, *105*, 671–683.

Boichu, M., L. Menut, D. Khvorostyanov, L. Clarisse, C. Clerbaux, S. Turquety, and P.-F. Coheur (2013), Inverting for volcanic SO_2 flux at high temporal resolution using spaceborne plume imagery and chemistry-transport modeling: The 2010 Eyjafjallajökull eruption case study, *Atmos. Chem. Phys.*, *13*, 8569–8584, doi:10.5194/acp-13-8569-2013.

Bursik, M. (2001), Effect of wind on the rise height of volcanic plumes, *Geophy. Res. Lett.*, *28*, 3621–3624.

Carn, S., A. Krueger, N. Krotkov, K. Yang, and K. Evans (2009), Tracking volcanic sulfur dioxide clouds for aviation hazard mitigation, *Nat. Hazards*, *51*, 325–343, doi:10.1007/s11069-008-9228-4.

Clarisse, L., P.-F. Coheur, A. J. Prata, D. Hurtmans, A. Razavi, T. Phulpin, J. Hadji-Lazaro, and C. Clerbaux (2008), Tracking and quantifying volcanic SO_2 with IASI, the September 2007 eruption at Jebel at Tair, *Atmos. Chem. Phys.*, *8*, 7723–7734, doi:10.5194/acp-8-7723-2008.

Clarisse, L., D. Hurtmans, A. J. Prata, F. Karagulian, C. Clerbaux, M. D. Mazière, and P.-F. Coheur (2010), Retrieving radius, concentration, optical depth, and mass of different types of aerosols from high-resolution infrared nadir spectra, *Appl. Opt.*, *49*(19), 3713–3722.

Clarisse, L., D. Hurtmans, C. Clerbaux, J. Hadji-Lazaro, Y. Ngadi, and P.-F. Coheur (2012), Retrieval of sulphur dioxide from the infrared atmospheric sounding interferometer (IASI), *Atmos. Meas. Tech.*, *5*, 581–594, doi:10.5194/amt-5-581-2012.

Clarisse, L., P.-F. Coheur, A. J. Prata, J. Hadji-Lazaro, D. Hurtmans, and C. Clerbaux (2013), A unified approach to infrared aerosol remote sensing and type specification, *Atmos. Chem. Phys.*, *13*(4), 2195–2221.

Clerbaux, C. A., et al. (2009), Monitoring of atmospheric composition using the thermal infrared IASI/MetOp sounder, *Atmos. Chem. Phys.*, *9*, 6041–6054, doi:10.5194/acp-9-6041-2009.

Dacre, H. F., A. L. M. Grant, and B. T. Johnson (2013), Aircraft observations and model simulations of particle size distribution in the Eyjafjallajokull volcanic ash cloud, *Atmos. Chem. Phys.*, *13*, 1277–1291.

Degruyter, W., and C. Bonadonna (2012), Improving on mass flow rate estimates of volcanic eruptions, *Geophy. Res. Lett.*, *39*, L16308, doi:10.1029/2012GL052566.

Durant, A. J., and W. I. Rose (2009), Sedimentological constraints on hydrometeor-enhanced particle deposition: 1992 eruptions of Crater Peak, Alaska, *J. Volcanol. Geotherm. Res*, *186*(1–2), 40–59, doi:10.1016/j.jvolgeores.2009.02.004.

Durant, A. J., C. Bonadonna, and C. J. Horwell (2010), Atmospheric and environmental impacts of volcanic particulates, *Elements*, *6*(4), 235–240.

Eckhardt, S., A. J. Prata, P. Seibert, K. Stebel, and A. Stohl (2008), Estimation of the vertical profile of sulfur dioxide injection into the atmosphere by a volcanic eruption using satellite column measurements and inverse transport modeling, *Atmos. Chem. Phys.*, *8*, 3881–3897.

Flemming, J., and A. Inness (2013), Volcanic sulfur dioxide plume forecasts based on UV-satellite retrievals for the 2011 Grímsvötn and the 2010 Eyjafjallajökull eruption, *J. Geophys. Res. Atmos.*, *118*, 1–18, doi:10.1002/jgrd.50753.

Gudmundsson, M. T., et al. (2012), Ash generation and distribution from the April-May 2010 eruption of Eyjafjallajökull, Iceland, *Sci. Rep.*, *2*, 572, doi:10.1038/srep00572.

Heim, M., B. J. Mullins, H. Umhauer, and G. Kasper (2008), Performance evaluation of three optical particle counters with an efficient "multimodal" calibration method, *Aerosol Sci. Technol.*, *39*(12), 1019–1031.

Holasek, R. E., A. W. Woods, and S. Self (1996), Experiments on gas-ash separation processes in volcanic umbrella plumes, *J. Volcanol. Geotherm. Res.*, *70*(3–4), 169–181, doi:10.1016/0377-0273(95)00054-2.

Horwell, C. J. (2007), Grain-size analysis of volcanic ash for the rapid assessment of respiratory health hazard, *J. Environ. Monit.*, *9*, 1107–1115, doi:1110.1039/b710583p.

Kerminen, V.-M., et al. (2011), Characterization of a volcanic ash episode in southern Finland caused by the Grímsvötn eruption in Iceland in May 2011, *Atmos. Chem. Phys.*, *11*, 12,227–12,239, doi:10.5194/acp-11-12227-2011.

Kristiansen, N. I., et al. (2010), Remote sensing and inverse transport modeling of the Kasatochi eruption sulfur dioxide cloud, *J. Geophys. Res.*, *115*, D00L16, doi:10.1029/2009JD013286.

Kristiansen, N. I., et al. (2012), Performance assessment of a volcanic ash transport model mini-ensemble used for inverse modeling of the 2010 Eyjafjallajökull eruption, *J. Geophys. Res.*, *117*, D00U11, doi:10.1029/2011JD016844.

Kvietkus, A., J. Šakalys, J. Didžbalis, I. Garbarienė, N. Špirkauskaitė, and V. Remeikis (2012), Atmospheric aerosol episodes over Lithuania after the May 2011 volcano eruption at Grímsvötn, Iceland, *Atmos. Res.*, *122*, 93–101.

Krueger, A. J., C. C. Schnetzler, and L. S. Walter (1996), The December 1981 eruption of Nyamuragira volcano (Zaire), and the origin of the "mystery cloud" of early 1982, *J. Geophys. Res.*, *101*, 15,191–15,196, doi:10.1029/96JD00221.

Lieke, K. I., T. B. Kristensen, U. S. Korsholm, J. H. Sørensen, K. Kandler, S. Weinbruch, D. Ceburnis, J. Ovadnevaite, C. D. O'Dowd, and M. Bilde (2013), Characterization of volcanic ash from the 2011 Grímsvötn eruption by means of single-particle analysis, *Atmos. Environ.*, *79*, 411–420.

Lopez, T., S. Carn, C. Werner, D. Fee, P. Kelly, M. Doukas, M. Pfeffer, P. Webley, C. Cahill, and D. Schneider (2012), Evaluation of Redoubt Volcano's sulfur dioxide emissions by the Ozone Monitoring Instrument, *J. Volcanol. Geotherm. Res.*, *259*, 290–307, doi:10.1016/j.jvolgeores.2012.03.002.

Mastin, L. G. (2007), A user-friendly one-dimensional model for wet volcanic plumes, *Geochem. Geophys. Geosyst.*, *8*, Q03014, doi:10.1029/2006GC001455.

Mastin, L. G., M. Guffanti, J. E. Ewert, and J. Spiegel (2009a), Preliminary spreadsheet of eruption source parameters for volcanoes of the world. Open-File Report, U.S. Geological Survey, 1133.

Mastin, L. G., et al. (2009b), A multidisciplinary effort to assign realistic source parameters to models of volcanic ash-cloud transport and dispersion during eruptions, *J. Volcanol. Geotherm. Res.*, *186*, 10–21.

Merucci, L., M. R. Burton, S. Corradini, and G. G. Salerno (2011), Reconstruction of SO_2 flux emission chronology from space-based measurements, *J. Volcanol. Geotherm. Res.*, *206*, 80–87.

Miller, T. P., and T. J. Casadevall (2000), Volcanic ash hazards to aviation, in *Encyclopedia of Volcanoes*, edited by H. Sigurdsson, pp. 915–930, Academic Press, San Diego, Calif.

Montopoli, M., G. Vulpiani, D. Cimini, E. Picciotti, and F. S. Marzano (2013), Interpretation of observed microwave signatures from ground dual polarization radar and space multi frequency radiometer for the 2011 Grímsvötn volcanic eruption, *Atmos. Meas. Tech. Discuss.*, *6*, 6215–6248, doi:10.5194/amtd-6-6215-2013.

Mosca, S., G. Graziani, W. Klug, R. Bellasio, and R. Bianconi (1998), A statistical methodology for the evaluation of long-range dispersion models: An application to the ETEX exercise, *Atmos. Environ.*, *32*(24), 4307–4324, doi:10.1016/S1352-2310(98)00179-4.

Naeslund, E., and L. Thaning (1991), On the settling velocity in a nonstationary atmosphere, *Aerosol Sci. Technol.*, *14*, 247–256.

Oberhuber, J. M., M. Herzog, H.-F. Graf, and K. Schwanke (1998), Volcanic plume simulation on large scales, *J. Volcanol. Geotherm. Res.*, *87*, 29–53, doi:10.1016/S0377-0273(98)00099-7.

Petersen, G. N., H. Bjornsson, P. Arason, and S. von Löwis (2012a), Two weather radar time series of the altitude of the volcanic plume during the May 2011 eruption of Grímsvötn, Iceland, *Earth Syst. Sci. Data*, *4*(1), 121–127, doi:10.5194/essd-4-121-2012.

Petersen, G. N., S. von Lowis, B. Brooks, J. Groves, and S. Mobbs (2012b), Utilising a LIDAR to detect volcanic ash in the near-field, *Weather*, *67*(6), 149–153, doi:10.1002/wea.1911.

Prata, A. J. (2008), Satellite detection of hazardous volcanic clouds and the risk to global air traffic, *Nat. Haz*, *51*, 303–324, doi:10.1007/s11069-008-9273-z.

Prata, A., and J. Kerkmann (2007), Simultaneous retrieval of volcanic ash and SO_2 using MSG-SEVIRI measurements, *Geophys. Res. Lett.*, *34*, L05813, doi:10.1029/2006GL028691.

Prata, A. J., and A. T. Prata (2012), Eyjafjallajökull volcanic ash concentrations determined from SEVIRI measurements, *J. Geophys. Res.*, *117*, D00U23, doi:10.1029/2011JD016800.

Prata, A. J., and A. Tupper (2009), Aviation hazards from volcanoes: The state of the science, *Nat. Hazards*, *51*, 239–244.

Robock, A. (2004), Climatic impact of volcanic emissions, in *State of the Planet: Frontiers and Challenges in Geophysics*, edited by A. Robock and C. Oppenheimer, pp. 125–134, AGU, Washington, D. C.

Schneider, D., W. Rose, L. Coke, and G. Bluth (1999), Early evolution of a stratospheric volcanic eruption cloud as observed with TOMS and AVHRR, *J. Geophys. Res.*, *104*, 4037–4050, doi:10.1029/1998JD200073.

Seibert, P. (2000), Inverse modeling of sulfur emissions in Europe based on trajectories, in *Inverse Methods in Global Biogeochemical Cycles*, *Geophys. Monogr.*, vol. 114, edited by P. Kasibhatla et al., pp. 147–154, AGU, Washington, D. C., doi:10.1029/GM114p0147.

Seibert, P., and A. Frank (2004), Source-receptor matrix calculation with a Lagrangian particle dispersion model in backward mode, *Atmos. Chem. Phys.*, *4*, 51–63.

Seibert, P., N. I. Kristiansen, S. Eckhardt, A. J. Prata, A. Richter, and A. Stohl (2011), Uncertainties in the inverse modelling of sulphur dioxide eruption profiles, *Geomath. Nat. Hazards Risk*, *2*, 201–216, doi:10.1080/19475705.2011.590533.

Sigmarsson, O., B. Haddadi, S. Carn, S. Moune, J. Gudnason, K. Yang, and L. Clarisse (2013), The sulfur budget of the 2011 Grímsvötn eruption, Iceland, *Geophys. Res. Lett.*, *40*, 6095–6100, doi:10.1002/2013GL057760.

Stohl, A., M. Hittenberger, and G. Wotawa (1998), Validation of the Lagrangian particle dispersion model FLEXPART against large-scale tracer experiment data, *Atmos. Environ.*, *32*, 4245–4264, doi:10.1016/S1352-2310(98)00184-8.

Stohl, A., C. Forster, A. Frank, P. Seibert, and G. Wotawa (2005), Technical note: The Lagrangian particle dispersion model FLEXPART version 6.2, *Atmos. Chem. Phys.*, *5*, 2461–2474.

Stohl, A., et al. (2011), Determination of time- and height-resolved volcanic ash emissions and their use for quantitative ash dispersion modeling: The 2010 Eyjafjallajökull eruption, *Atmos. Chem. Phys.*, *11*, 4333–4351, doi:10.5194/acp-11-4333-2011.

Sparks, R. S. J., M. I. Bursik, S. N. Carey, J. S. Gilbert, L. S. Glaze, H. Sigurdsson, and A. W. Woods (1997), *Volcanic Plumes*, 574 pp., John Wiley, Chichester, U. K.

Tesche, M., P. Glantz, C. Johansson, M. Norman, A. Hiebsch, A. Ansmann, D. Althausen, R. Engelmann, and P. Seifert (2012), Volcanic ash over Scandinavia originating from the Grímsvötn eruptions in May 2011, *J. Geophys. Res.*, *117*, D09201, doi:10.1029/2011JD017090.

Textor, C., H.-F. Graf, M. Herzog, and J. M. Oberhuber (2003), Injection of gases into the stratosphere by explosive volcanic eruptions, *J. Geophys. Res.*, *108*(D19), 4606, doi:10.1029/2002JD002987.

Theys, N., et al. (2013), Volcanic SO_2 fluxes derived from satellite data: A survey using OMI, GOME-2, IASI and MODIS, *Atmos. Chem. Phys.*, *13*, 5945–5968.

Thomas, H. E., and A. J. Prata (2011), Sulphur dioxide as a volcanic ash proxy during the April-May 2010 eruption of Eyjafjallajökull Volcano, Iceland, *Atmos. Chem. Phys.*, *11*, 6871–6880, doi:10.5194/acp-11-6871-2011.

Thorsteinsson, T., T. Jóhannsson, A. Stohl, and N. I. Kristiansen (2012), High levels of particulate matter in Iceland due to direct ash emissions by the Eyjafjallajökull eruption and resuspension of deposited ash, *J. Geophys. Res.*, *117*, B00C05, doi:10.1029/2011JB008756.

Weber, K., J. Eliason, A. Vogel, C. Fischer, T. Pohl, G. van Haren, M. Meier, B. Groberty, and D. Dahmann (2012a), Airborne in-situ investigations of the Eyjafjallajökull volcanic ash plume on Iceland and over north-western Germany with light aircrafts and optical particle counters, *Atmos. Environ.*, *48*, 9–21.

Weber, K., R. Reichardt, A. Vogel, C. Fischer, H. M. Moser, and J. Eliasson (2012b), Computational visualization of volcanic ash plume concentrations measured by light aircrafts over Germany and Iceland during the recent eruptions of the volcanoes Eyjafjallajökull and Grímsvötn, in *Recent Advances in Fluid Mechanics, Heat & Mass Transfer, Biology and Ecology*, edited by M. K. Jha et al., pp. 236–240, World Scientific and Engineering Academy and Society, Harvard, Cambridge.

Winker, D. M., M. A. Vaughan, A. Omar, Y. Hu, K. A. Powell, Z. Liu, W. H. Hunt, and S. A. Young (2009), Overview of the CALIPSO mission and CALIOP data processing algorithms, *J. Atmos. Oceanic Technol.*, *26*, 2310–2323, doi:10.1175/2009JTECHA1281.1.

Woodhouse, M. J., A. J. Hogg, J. C. Phillips, and R. S. J. Sparks (2013), Interaction between volcanic plumes and wind during the 2010 Eyjafjallajökull eruption, Iceland, *J. Geophys. Res. Solid Earth*, *118*, 92–109, doi:10.1029/2012JB009592.